COAT/TARGET-SIGNATURE INTERACTIONS

HUGHES RESEARCH LABORATORIES

PREPARED FOR
ROME AIR DEVELOPMENT CENTER

APRIL 1976

RADC-TR-76-64
Technical Report
April 1976

COAT/TARGET-SIGNATURE INTERACTIONS

Hughes Research Laboratories

Sponsored By
Defense Advanced Research Projects Agency
ARPA Order No. 1279

Approved for public release;
distribution unlimited.

ROME AIR DEVELOPMENT CENTER
AIR FORCE SYSTEMS COMMAND
GRIFFISS AIR FORCE BASE, NEW YORK 13441

This report has been reviewed by the RADC Information Office (OI) and is releasable to the National Technical Information Service (NTIS). At NTIS it will be releasable to the general public, including foreign nations.

This report has been reviewed and approved for publication.

APPROVED: Robert F. Ogrodnik

ROBERT F. OGRODNIK
Project Engineer

The views and conclusions contained in this document are those of the authors and should not be interpreted as necessarily representing the official policies, either expressed or implied, of the Defense Advanced Research Projects Agency or the U. S. Government.

Do not return this copy. Retain or destroy.

UNCLASSIFIED

SECURITY CLASSIFICATION OF THIS PAGE (When Data Entered)

REPORT DOCUMENTATION PAGE		READ INSTRUCTIONS BEFORE COMPLETING FORM
1. REPORT NUMBER RADC-TR-76-64	2. GOVT ACCESSION NO.	3. RECIPIENT'S CATALOG NUMBER
4. TITLE (and Subtitle) COAT/TARGET-SIGNATURE INTERACTIONS		5. TYPE OF REPORT & PERIOD COVERED Interim Report 1 Aug 75 - 31 Oct 75
		6. PERFORMING ORG. REPORT NUMBER N/A
7. AUTHOR(s) M. E. Pedinoff S. A. Kokorowski J. E. Pearson		8. CONTRACT OR GRANT NUMBER(s) F30602-75-C-0021
9. PERFORMING ORGANIZATION NAME AND ADDRESS Hughes Research Laboratories 3011 Malibu Canyon Road Malibu CA 90265		10. PROGRAM ELEMENT, PROJECT, TASK AREA & WORK UNIT NUMBERS 62301E 12790020
11. CONTROLLING OFFICE NAME AND ADDRESS Defense Advanced Research Projects Agency 1400 Wilson Blvd Arlington VA 22209		12. REPORT DATE April 1976 13. NUMBER OF PAGES 74
14. MONITORING AGENCY NAME & ADDRESS(if different from Controlling Office) Rome Air Development Center (OCTM) Griffiss AFB NY 13441		15. SECURITY CLASS. (of this report) UNCLASSIFIED 15a. DECLASSIFICATION/DOWNGRADING SCHEDULE N/A

16. DISTRIBUTION STATEMENT (of this Report)

Approved for public release; distribution unlimited.

17. DISTRIBUTION STATEMENT (of the abstract entered in Block 20, if different from Report)

Same

18. SUPPLEMENTARY NOTES

RADC Project Engineer:
Robert F. Ogrodnik (OCTM)

19. KEY WORDS (Continue on reverse side if necessary and identify by block number)

COAT, Speckle, Target Signature Effects, Laser Phased Arrays, Active Optics, Adaptive Systems

20. ABSTRACT (Continue on reverse side if necessary and identify by block number)

Target speckle modulation effects have been investigated experimentally using a number of scaled realistic targets with different shapes and surface textures, and analytically using theoretical target signature models (some generated by General Research Corporation (GRC)) in a computer simulation model of a multi-dither COAT system. The experimental results have shown that maximum contrast ratios of 0.79 can occasionally be obtained, but that the average is much lower. Significant receiver aperture integration effects cause reduction of the contrast ratio. Temporal frequency spectra obtained by rotation of the targets

DD FORM 1 JAN 73 1473 EDITION OF 1 NOV 65 IS OBSOLETE

UNCLASSIFIED

SECURITY CLASSIFICATION OF THIS PAGE (When Data Entered)

agree with spatial frequency data obtained by fast Fourier transform processing of the target signature data. Preliminary computer simulation results using high contrast ratio spackle data from GRC show degraded COAT system performance. The severity of the degradation has been attributed in part to: (1) unrealistically harsh assumptions in the GRC speckle model including assumption of a point receiver, and an inadequate sampling of the speckle waveform; (2) several discrepancies between the real COAT system and the computer simulation model, especially in the automatic gain control portion of the system. A preliminary adjustment of the COAT simulation model has led to reduced susceptibility to high contrast speckle modulation. In addition, theoretical arguments, corroborated by our experimental results, indicate that such high contrast ratios are not realistic at visible wavelengths.

COAT/TARGET-SIGNATURE INTERACTIONS

M. E. Pedinoff
S. A. Kokorowski
J. E. Pearson

Contractor: Hughes Research Laboratories
Contract Number: F30602-76-C-0021
Effective Date of Contract: 1 August 1975
Contract Expiration Date: 30 June 1976
Amount of Contract: $100,000.00
Program Code Number: 6E20
Period of work covered: Aug 75 - Oct 75

Principal Investigator: J. E. Pearson
Phone: 213 456-6411

Project Engineer: Robert F. Ogrodnik
Phone: 315 330-4306

Approved for public release;
distribution unlimited.

This research was supported by the Defense Advanced Research Projects Agency of the Department of Defense and was monitored by Robert F. Ogrodnik (OCTM), Griffiss AFB NY 13441.

PREFACE

This interim report was prepared by Hughes Research Laboratories, Malibu, California under contract F30602-76-C-0021. It describes work performed from 1 August 1975 to 31 October 1975. The principal scientist is Dr. James E. Pearson and the principal investigators are Dr. Melvin E. Pedinoff and Mr. Stan A. Kokorowski. This project is a part of the Adaptive Optics program in the Opto-Electronics Department, managed by Dr. Viktor Evtuhov, at Hughes Research Laboratories.

SUMMARY

The objectives of this program are threefold: (1) to determine what kind of modulations interfere with the proper operation of a multi-dither COAT system and to characterize the amplitude, frequency spectrum and spectral power density of these modulations; (2) to determine the characteristics of receiver modulations produced by backscatter from real targets in expected operational scenarios and to assess their effectiveness in degrading COAT system convergence and performance; (3) to determine an optimum COAT system design that is insensitive to speckle induced receiver modulati nd to define the critical design parameters. This report summarizes the w k performed from 1 August 1975 to 31 October 1975.

We have experimentally studied the speckle patterns generated by scaled realistic target models consisting of metallized or painted spheres, cylinders, and cones using a helium-neon (6328 Å) target-speckle measurement apparatus specifically assembled for this program. Target signatures were recorded with two receiver apertures, one equal to the transmitter aperture, and one equal to one-third of the transmitter aperture. The larger aperture size significantly reduces the observed speckle contrast ratio and reduces the amplitude of the higher speckle spatial frequency components.

Speckle pattern data and fast-Fourier-transform spatial frequency spectra obtained by rotation of the target, or by translation of the receiver, have proven to be identical in the study, thus simplifying the remaining experimental tasks in this program.

Target speckle signatures taken with most of the metallized target shapes are very similar, with the exception of a cone-shaped target illuminated nose-on. This target showed a very broad speckle pattern due to the small scattering cross section of the nose. Experiments with white painted (Lambertian scattering) targets showed reduced contrast ratios due to decorrelation of the two orthogonally polarized speckle patterns.

The maximum contrast ratio observed in all of the experiments was 0.89 and the average of all of the maximum contrast ratios was 0.56. The average contrast ratios observed were considerably lower and are estimated to be approximately 60% of these figures.

Real time spectrum analyzer spectra obtained by rapid rotation of the targets are identical to spatial frequency spectra obtained by performing a fast Fourier transform (FFT) on the speckle pattern data. Increasing the target rotation speed caused the speckle spectrum to broaden toward high frequencies in agreement with the FFT spatial frequency results. The speckle signatures produced by rotation of the metallized targets are identical with those produced on an earlier program (contract F30602-75-C-0001) by rotating scotchlite targets. Since those targets failed to produce severe degradation of COAT system performance, the targets measured and reported here are expected to have little effect on system performance.

A statistical analytical model of speckle effects in multidither COAT systems has been developed. The model has shown that the ac signal power generated by speckle in the receiver can not exceed 0.5 times the dc power. A speckle amplitude coefficient C_s has been defined, equal to the square root of the ac speckle signal power, and the extreme of convergence as a function of speckle coefficient has been calculated for comparison with computer simulation results.

Computer simulations of multidither COAT performance have been made using an ad hoc "speckle" spectrum and using theoretical target speckle data generated by General Research Corporation. Three simulations were run corresponding to rotation of a uniformly illuminated spherical target at rates of 0.01, 2, and 10 rad sec. The corresponding speckle coefficients in our analysis are 0.04, 0.6, and 0.5. The latter two cases are sufficiently close to the largest possible speckle modulation coefficient of 0.707 to constitute worst cases. The response of an 18-channel COAT system was partially degraded at 0.01 rad/sec, and severely degraded for the other two cases. Investigation of the COAT computer model revealed significant second harmonic generation in the AGC at 65% modulation depth. This AGC

model was determined to be unrealistic. An improved AGC model in the simulation led to good agreement between computer-predicted convergence levels and those experimentally observed with the DARPA/RADC COAT system. The simulation model is not finalized, since at the moment it predicts longer convergence times with these changes than without them. By comparing the statistical analysis to the simulation results, we have found that the statistical analysis serves as a good predictor of the lower level of system convergence.

During the remainder of this program, experimental measurements will be performed with the DARPA/RADC COAT system on the speckle-characterized targets under conditions of thermal blooming and turbulence. An acousto-optic speckle simulation experiment will provide data on the minimum modulation index required to disable a single COAT servo channel. Work on the computer simulation model, in conjunction with the General Research Corporation, will continue throughout the remainder of the program.

TABLE OF CONTENTS

LIST OF ILLUSTRATIONS

I. INTRODUCTION

A. Program Objectives

The overall purpose of this program is to produce a consistent, unified theory on multidither COAT/target interactive effects that correlate experimental data with analytical models. Specifically there are three primary objectives. The first objective is to determine what kind of modulations interfere with the proper operation of a multidither COAT system. The significant parameters of the modulation are amplitude, frequency spectrum, and power spectral density. The second objective is to determine the characteristics of receiver modulations produced by backscatter from real targets in expected operational scenarios; that is, to determine which scenarios can produce the modulations which will affect the COAT system. The third objective is to determine an optimum COAT system design that is insensitive to speckle-induced receiver modulations and to define the critical design parameters.

B. Research Program Plan

The 18-element multidither COAT system developed and tested on DARPA/RADC Contract F30602-73-C-0248 was expanded to a 21-element system to include autotracking and focus controls under Amendment No. 1 of DARPA/RADC Contract F30602-75-C-0001. This same system is used for laboratory experiments on this program, which is an in-depth investigation of speckle phenomena.

The research program for this contract, illustrated in Figure 1, runs from 1 August 1975 to 1 February 1976. Because of ongoing measurements on the COAT Measurements and Analysis program, a separate target-speckle measurement apparatus was planned including a helium neon 6328 Å target illumination system.

The program is divided into three tasks: Target Backscatter Measurements, COAT System Measurements, and Analytical Studies. Task 1 represents the acquisition and characterization of targets and target speckle data not previously available to the program. Task 2 will determine COAT system performance in the presence of turbulence, blooming, and speckle noise modulation from these targets. Task 3 is a computer simulation study designed to corroborate or predict the experimental findings.

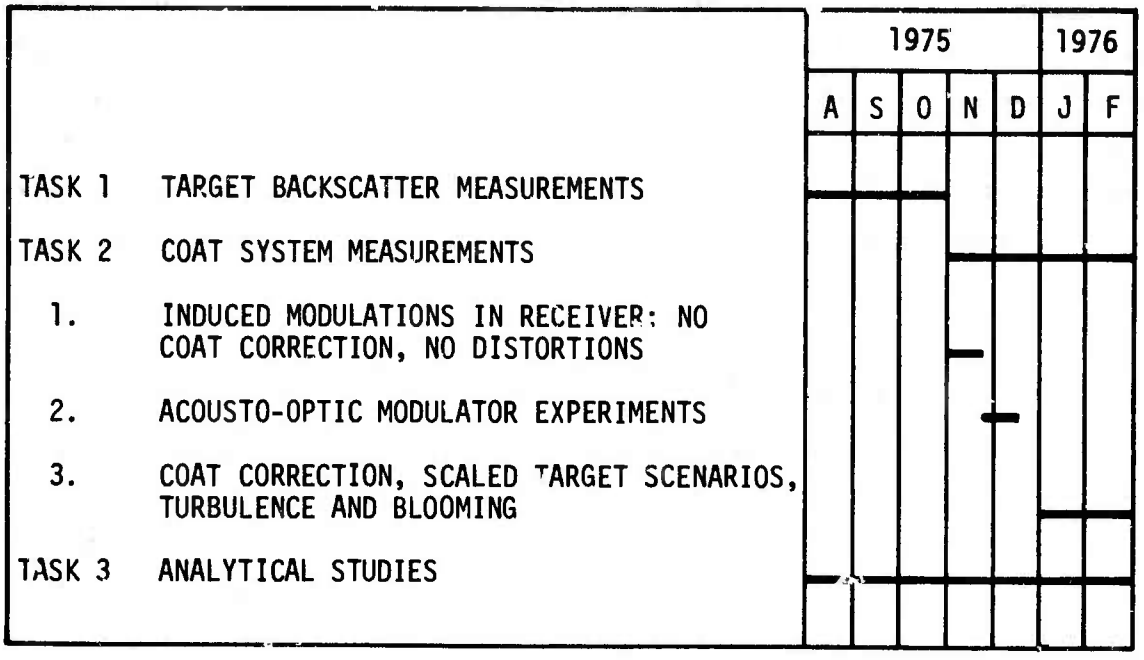

Figure 1. COAT/Target-Signature interaction schedule

II. SPECKLE AND TARGET SIGNATURES

The physical problem known as "speckle noise" can be stated briefly. When a coherent laser beam illuminates a target, some of the energy is scattered back in the direction of the transmitted beam. The backscattered radiation produces a random intensity pattern (a "speckle pattern") at a receiver, which is located close to the transmitter for cases of interest to us. When the appropriate conditions exist, any movement of this speckle pattern relative to the receiver will produce an amplitude modulation of the received signal. Since a multidither COAT system receiver senses amplitude modulations on the backscattered beam that are produced by dithering the transmitted beam phase, spurious amplitude modulations in the receiver may swamp the desired modulations and thus interfere with the system operation.

Doppler shifts produced by rapidly rotating targets may also produce false signals, but these spurious signals are expected to be less important than amplitude modulation effects for the target scenarios of interest. This is true because the most likely glint point on a rapidly rotating target is one normal to the beam incidence direction; this point will have nearly zero transverse doppler shift. Longitudinal doppler shifts are very narrow band and thus will have minimal effect on a multiple-channel COAT system.

The speckle characteristics of greatest interest to this program are the speckle contrast ratio and the spatial frequency spectrum of the speckle because these parameters can be directly translated into modulation depth and temporal frequency spectra for moving targets. These parameters are discussed in this section in terms of both analytical models and experimental measurements.

A. Analytical Speckle Models

1. Models for Transmissive Diffusers

In the analytical speckle theory derived by George, et al.,[1] a contrast ratio, C_R, is defined by the ratio of the standard deviation of the speckle intensity to the average intensity:

$$C_R = \frac{\sigma(u_x)}{\{u_x\}} = \frac{\left[\{u_x^2\} - \{u_x\}^2\right]^{\frac{1}{2}}}{\{u_x\}} \quad , \tag{1}$$

where the expected value of the intensity is $\{u_x\}$ and $\sigma(x)$ is its standard deviation. (In the analysis of the experimental results presented later in this report, a heuristic contrast ratio C_{R_1}, was used

$$C_{R_1} = \frac{u_{xi} - u_{xj}}{u_{xi} + u_{xj}} \tag{2}$$

where u_{xi} and u_{xj} are the instantaneous adjacent maximum and minimum values of a speckle intensity pattern. This datum represented the maximum contrast ratio observed in each experiment.)

In this theory, a transmissive diffuser with total surface proportional to A generates a specular transmission scattering term A-BN and a roughness term BN. Thus the electric field received at X in the image plane is given by

$$v(X) = A\text{-}BN + B \sum_{m=1}^{N} e^{-i \eta h_m} \quad , \tag{3}$$

where h_m represents the random height within the element and η represents the normalized radian frequency variable (phase variable). In the absence

of roughness all $h_m \equiv 0$ and $v(X) = A$. In the absence of specular behavior, the maximum value of BN is A. In general, the specular fraction is given by

$$S = \frac{A - BN}{A} \quad , \tag{4}$$

and the diffuse fraction is given by

$$b = \frac{BN}{A} \quad . \tag{5}$$

For the special case of a very rough surface, George's expression for the contrast ratio reduces to

$$C_R = \frac{\left\{ b^2 \frac{\left[2S^2 + b^2 \frac{(N-1)}{N^2} \right]}{N} \right\}^{\frac{1}{2}}}{\left(\frac{S^2 + b^2}{N} \right)} \tag{6}$$

Thus the contrast ratio for a very rough surface depends only on the diffuse fraction, b, the specular fraction S, and the total number of scatterers N, and not on the detailed density function for height $f(h_m)$

For the nonspecular case, $S = 0$ ($b = 1$) and the contrast is 1. A more general calculation of the contrast ratio as a function of a frequency roughness parameter $\eta h/\pi$ is shown in Fig. 2. The variable h is the root mean square height of the diffuser and the parameter η is a normalized radian frequency variable. In effect, η is the average wave number differential encountered by the light in passing through the phase screen (diffuser). Thus the product $\eta h/\pi$ for the random phase screen is identical to a surface roughness parameter, h/λ, for reflection-generated speckle.

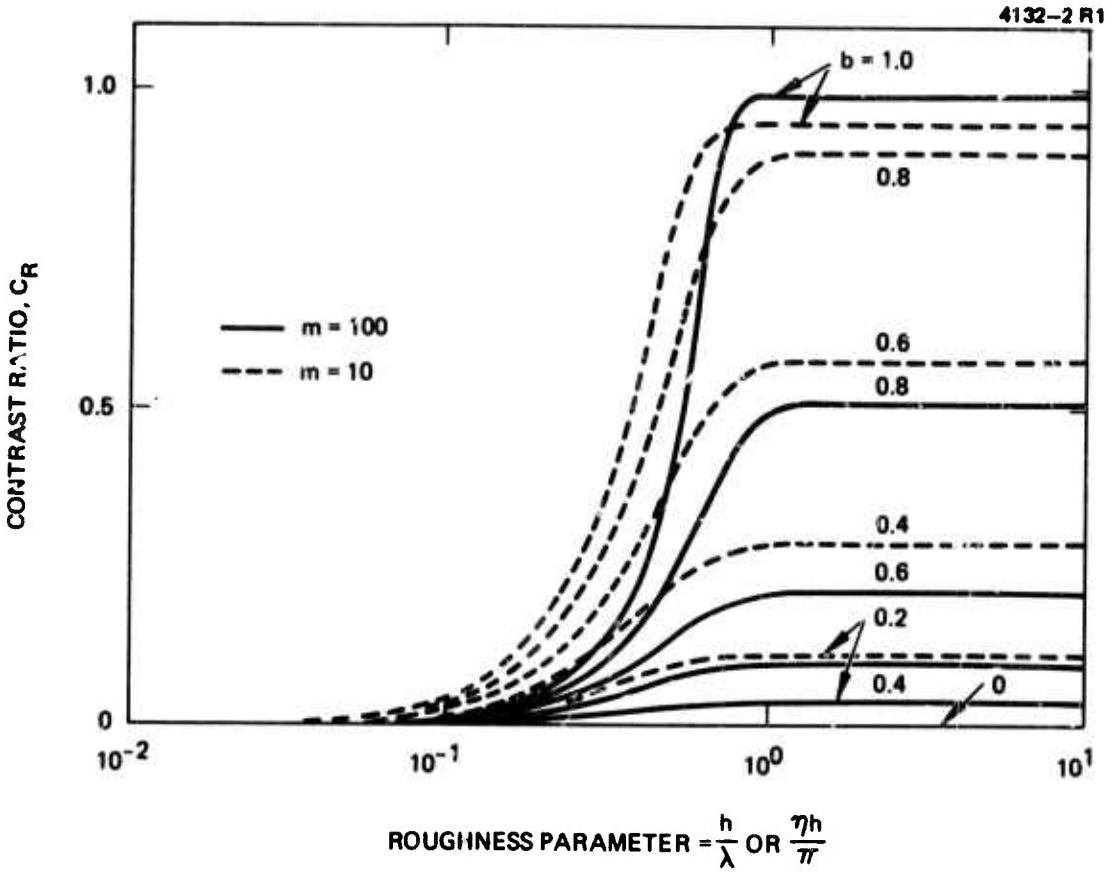

Figure 2. Contrast ratio C_R versus surface roughness parameter. The fractional diffuse reflectivity component is b where s+b = 1 (eq. 21)). The number of illuminated scatterers is m.

Several important conclusions can be derived from Fig. 2. First, for a large number of scatterers (m greater than or equal to 100), the specular component need only be increased to 20% (b = 0.8) to reduce the contrast ratio to 0.5. Second, for fixed values of b, increasing m almost always decreases the contrast ratio. The limited exception is the case b = 1, $h/\lambda > 0.5$ where a slight increase in contrast ratio occurs. Finally, for a given surface, as the wavelength increases, the contrast ratio decreases sharply when λ exceeds h. These results, combined with the fact that surfaces tend to become more specular (smaller values of b in Fig. 2) at longer wavelengths, indicate that speckle modulation effects will be less severe at 10.6 μm or 3.8 μm than at 0.5 μm.

2. Probability Density Model of Speckle

From J.M. Burch,[2] the probability density function $P_x(u_x)$ for a speckle intensity u_x containing a specular component is given by

$$P_x(u_x) = \frac{1}{\bar{u}_x\left(1 - \sqrt{1 - C_R^2}\right)} \exp\left[\frac{-\left(u_x + \bar{u}_x\sqrt{1 - C_R^2}\right)}{\bar{u}_x\left(1 - \sqrt{1 - C_R^2}\right)}\right]$$

$$\cdot I_o\left[\frac{2\left(u_x \bar{u}_x \sqrt{1 - C_R^2}\right)^{\frac{1}{2}}}{\bar{u}_x\left(1 - \sqrt{1 - C_R^2}\right)}\right] , \qquad (7)$$

where $\bar{u}_x$ is the mean of intensity, C_R is the contrast ratio defined as the ratio of the standard deviation of intensity σ to the mean $\bar{u}_x$, i.e. $C_R = \sigma/\bar{u}_x$. The function I_o is the modified Bessel's function of order zero. One finds that for $C_R = 1$, the density function reduces to

$$P_x(u_x) = \frac{1}{u_x} \exp\left(\frac{-u_x}{\bar{u}_x}\right) . \qquad (8)$$

This result signifies that at zero intensity, $u_x/\bar{u}_x = 0$, and for high contrast ratios the probability density of zero intensity is not zero. In other terms, in the absence of a specular component the special case $C_R = 1$ occurs, and there is a high probability of finding an intensity zero (null) in the speckle pattern.

For unpolarized or depolarized Lambertian scattering, the speckle intensity u is the sum of the intensities of 2 orthogonal polarizations $u_x + u_y$ which are uncorrelated. The density P_o for the total intensity is calculated from a convolution of P_x and P_y.

$$P_o(u) = \int_o^u P_x(u - u_y)\, P_y(u_y)du_y \quad . \tag{9}$$

The quantities $P_o(u)$ and $P_x(u_x)$ in eqs. (7) and (9) are plotted in Figs. 3(a) and 3(b). The contrast ratios used to produce the curves in Fig. 3 were taken from experimental measurements on a series of diffusers of varying thickness by George, et al.[1] A very significant conclusion that can be drawn from Fig. 3(a) for a surface roughness corresponding to or greater than 100 μm diffuser thickness, is a large probability density at zero intensity. That is, the polarized speckle patterns will have deep nulls and contrast ratios of 1. For smaller surface roughness, the contrast ratio will be less than 1. In Fig. 3(b), which is for unpolarized scatterings (as from a Lambertian surface), contrast ratios of 1 are found only for a narrow range of the roughness corresponding to a diffuser thickness of 100 μm.

One can conclude from these results that contrast ratios of 1 will be observed occasionally with polarized receivers when the surface roughness is large, and contrast ratios less than 1 will occur with unpolarized receivers. This conclusion is valid, however, only for targets which produce significant depolarization of the backscattered energy. In visible wavelength experiments, Lambertian scatterers usually exhibit this behavior. Such depolarization, however, may not apply at 3.8 or 10.6 μm wavelengths. We must also be

This result signifies that at zero intensity, $u_x/\bar{u}_x = 0$, and for high contrast ratios the probability density of zero intensity is not zero. In other terms, in the absence of a specular component the special case $C_R = 1$ occurs, and there is a high probability of finding an intensity zero (null) in the speckle pattern.

For unpolarized or depolarized Lambertian scattering, the speckle intensity u is the sum of the intensities of 2 orthogonal polarizations $u_x + u_y$ which are uncorrelated. The density P_o for the total intensity is calculated from a convolution of P_x and P_y.

$$P_o(u) = \int_o^u P_x(u - u_y)\, P_y(u_y)\, du_y \quad . \tag{9}$$

The quantities $P_o(u)$ and $P_x(u_x)$ in eqs. (7) and (9) are plotted in Figs. 3(a) and 3(b). The contrast ratios used to produce the curves in Fig. 3 were taken from experimental measurements on a series of diffusers of varying thickness by George, et al.[1] A very significant conclusion that can be drawn from Fig. 3(a) for a surface roughness corresponding to or greater than 100 μm diffuser thickness. is a large probability density at zero intensity. That is, the polarized speckle patterns will have deep nulls and contrast ratios of 1. For smaller surface roughness, the contrast ratio will be less than 1. In Fig. 3(b), which is for unpolarized scatterings (as from a Lambertian surface), contrast ratios of 1 are found only for a narrow range of the roughness corresponding to a diffuser thickness of 100 μm.

One can conclude from these results that contrast ratios of 1 will be observed occasionally with polarized receivers when the surface roughness is large, and contrast ratios less than 1 will occur with unpolarized receivers. This conclusion is valid, however, only for targets which produce significant depolarization of the backscattered energy. In visible wavelength experiments, Lambertian scatterers usually exhibit this behavior. Such depolarization, however, may not apply at 3.8 or 10.6 μm wavelengths. We must also be

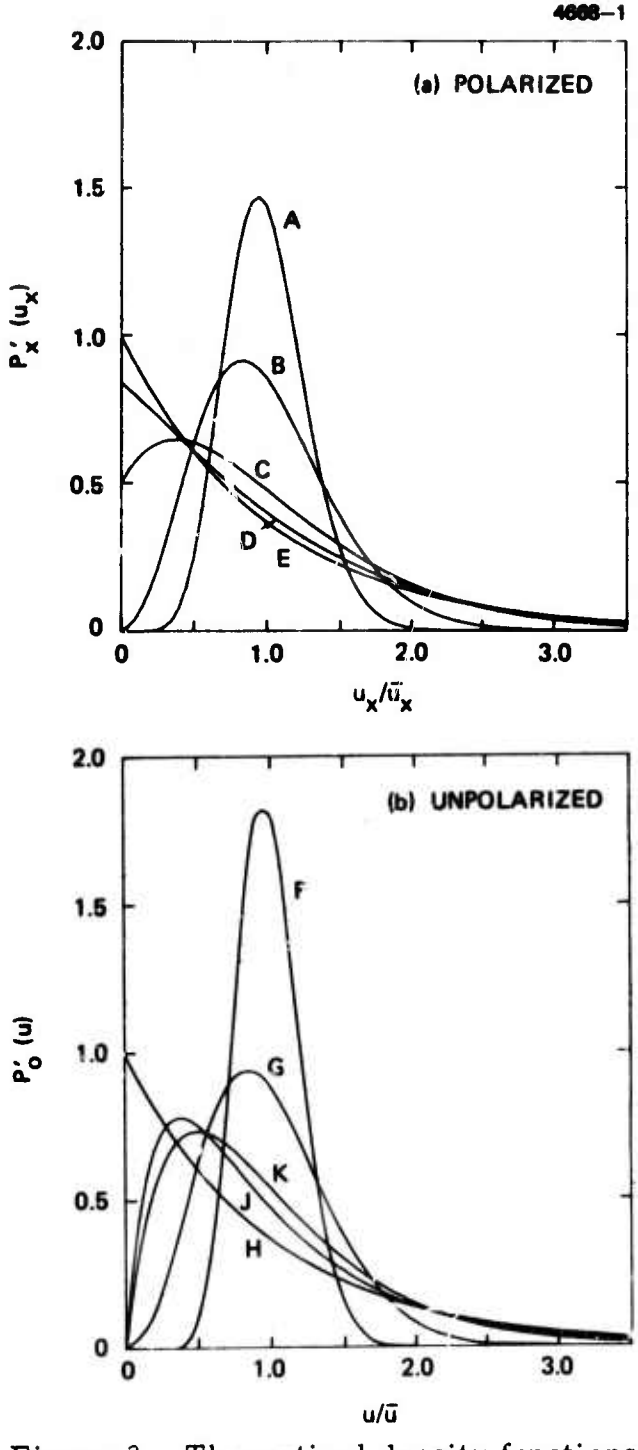

Figure 3. Theoretical density functions for polarized and unpolarized speckle intensity. A, F - 25 μm diffuser; B, G - 50 μm diffuser; C, H - 100 μm diffuser; D, J - 200 μm; E, K - 500 μm.

careful when drawing conclusions from data based on transmissive scatterers; reflective targets can exhibit quite different properties. In particular, depolarization and "diffuse" scattering* are not necessarily coupled for reflective targets.

3. Spatial Frequency Spectra of Speckle

The spatial frequency spectrum of speckle is proportional to the autocorrelation of the squared amplitude of the illumination function. For this scenario, i.e., target illumination with a Gaussian beam, the autocorrelation is also Gaussian but of twice the width. It has been shown by N. George[3] that the spatial frequency distribution (or power density) of speckle for the one dimensional case is given by

$$S(f_x) \propto A^2(0)\,\delta(f_x)\,\lambda r_o + (\lambda r_o)^2 \left| a(\lambda, r_o, f_x)\right|^2 * \left| a(\lambda, r_o, f_x)\right|^2 \qquad (10)$$

where * denotes the autocorrelation with respect to the spatial frequency variable f_x, λ is the optical wavelength and r_o is the target range. In the lefthand term, $A^2(0)$ represents the total power in the illuminating beam and the function $a(\lambda, r_o, f_x)$ represents the amplitude distribution in the illuminating beam. In the present investigation, the illumination intensity is Gaussian of the form

$$I(X) = e^{-\frac{1}{2}\frac{X^2}{\sigma^2}} \equiv \left| a(X)\right|^2 \quad . \qquad (11)$$

*By "diffuse" we mean a target that completely randomizes the phase of an optical wave incident on it, not necessarily a wide-angle or Lambertian scatterer.

The autocorrelation function of this Gaussian is also a Gaussian of twice the width given by

$$I(X) * I(X) = \sigma\sqrt{\pi}\, e^{-\frac{X^2}{4\sigma^2}} \quad . \tag{12}$$

Substituting the transformation variable for X one obtains for the spectrum

$$S(f_x) = A_0^2\, \delta(f_x)\lambda r_o + \lambda r_o\, \sigma\sqrt{\pi}\, e^{-\left(\frac{\lambda r_o f_x}{2\sigma}\right)^2} \quad , \tag{13}$$

where $\sigma \cong 0.42$ times the full width at half maximum of the Gaussian beam. Using the experimental values $\sigma = 2.8 \times 10^{-3}$ m, $\lambda = 0.633 \times 10^{-6}$ μm, and $r_o = 1.8$ m, we obtain the amplitude and power spectrum results shown in Fig. 4. When finite aperture averaging from a 0.15 mm aperture is used to weight the speckle spectrum, the lower curves result. We will see later that these spatial frequency spectra are fairly accurate representations of measured phenomena.

B. Experimental Speckle Measurements

Experimental measurements at Caltech are shown in Support of the theory by George et al.[1] in Figs. 5(a) and 5(b). The general features of the theoretical curves in Fig. 3 and the experimental curves in Fig. 5 are in excellent agreement. The polarized receiver case with the 500 μm diffuser shows a contrast ratio of 1 as expected. A simple summary of the thick diffuse experimental speckle measurements is presented in Fig. 6. For our purpose, the diffuser thickness can be likened to surface roughness. For the unpolarized receiver case, the contrast ratio is always less than 1 and drops to 0.5 for large thickness (roughness). The maximum contrast ratio of 0.9 occurs at a diffuser thickness of 100 μm and falls off on either side for the unpolarized case. For reflective targets, this is equivalent to the statement

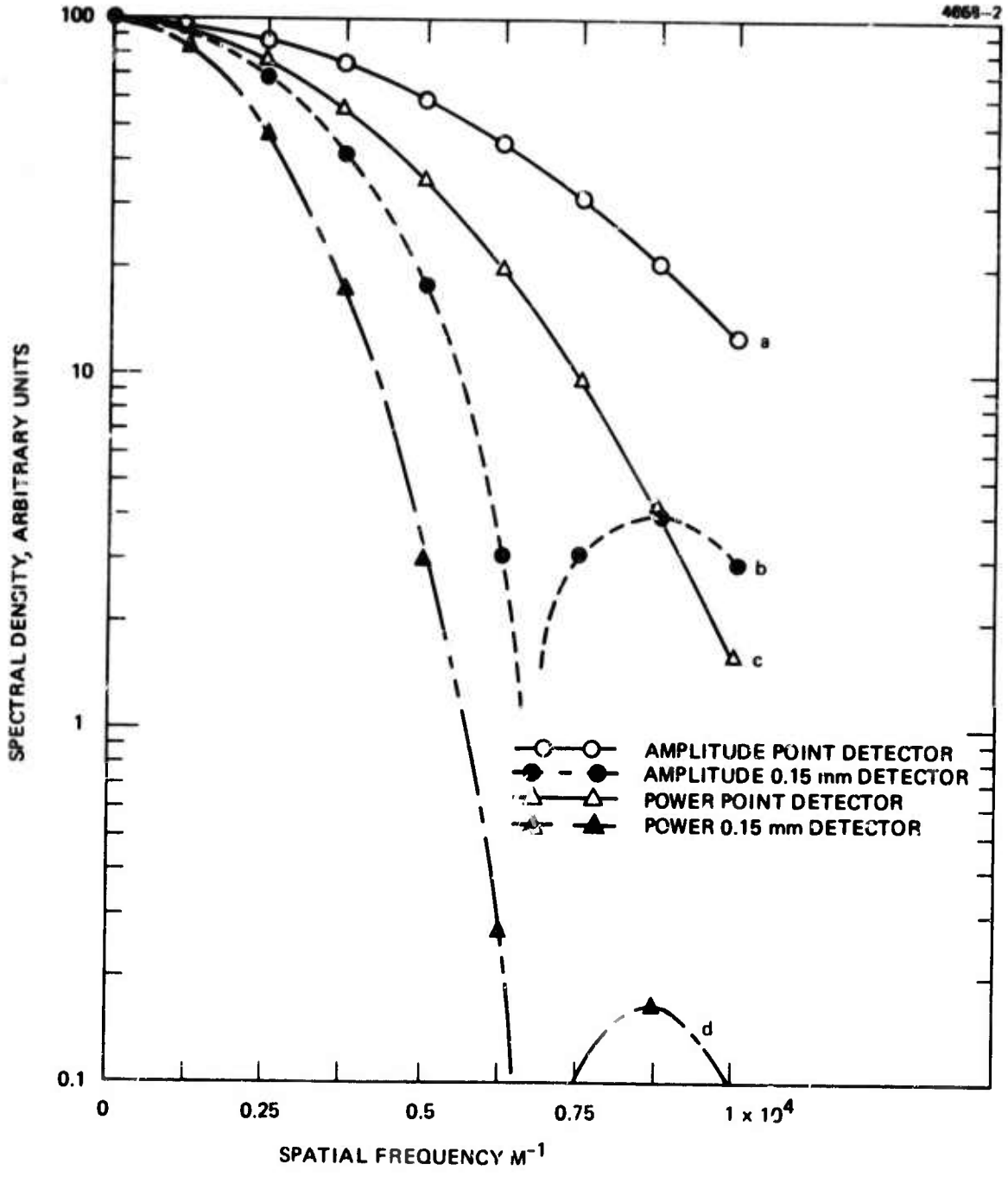

Figure 4. Theoretical spatial frequency spectra of speckle with Gaussian illumination. (a) Amplitude spectrum with point detector, (b) Amplitude spectrum with 0.15 mm detector, (c) Power spectrum with point detector, and (d) Power spectrum with 0.15 mm detector.

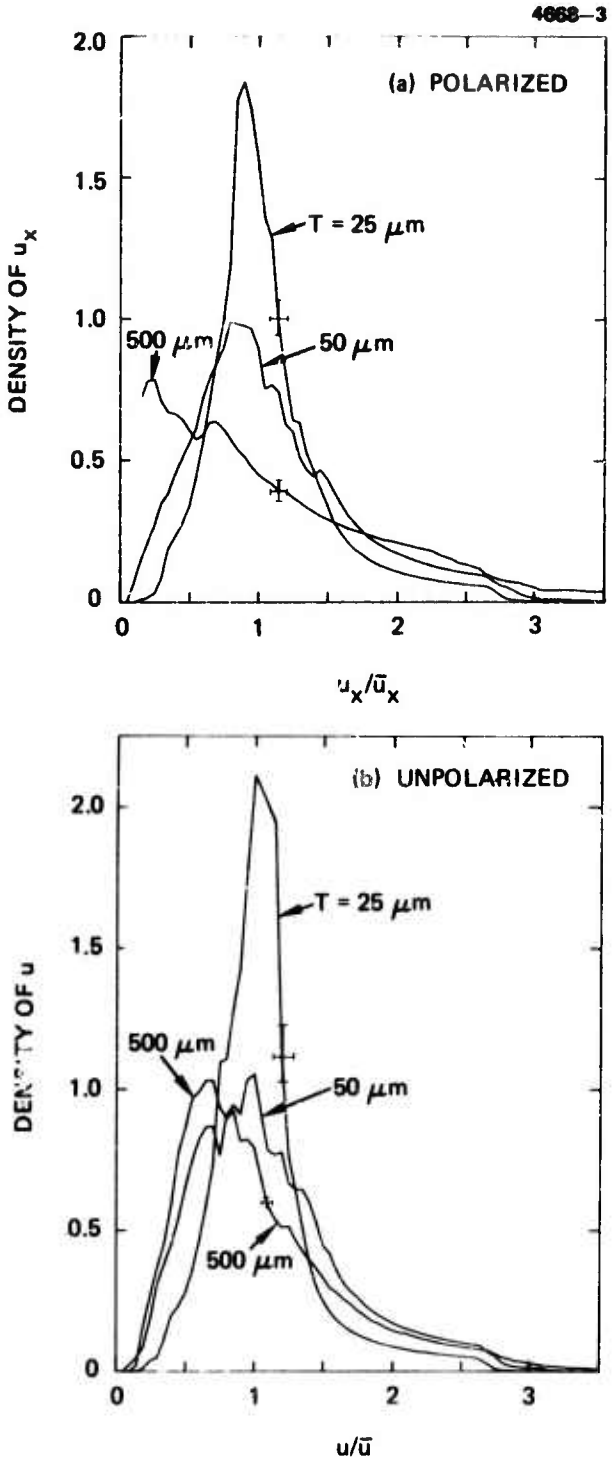

Figure 5. Experimental density functions for polarized and unpolarized light as for several diffuser thicknesses.

made earlier; when a statistical distribut n of surface roughness exists, and whe. the target has Lambertian characteristics, the unpolarized contrast ratio will always be less than 0.9. Moreover, the contrast ratio will be lower at longer wavelengths if the reflection characteristics become more specular.

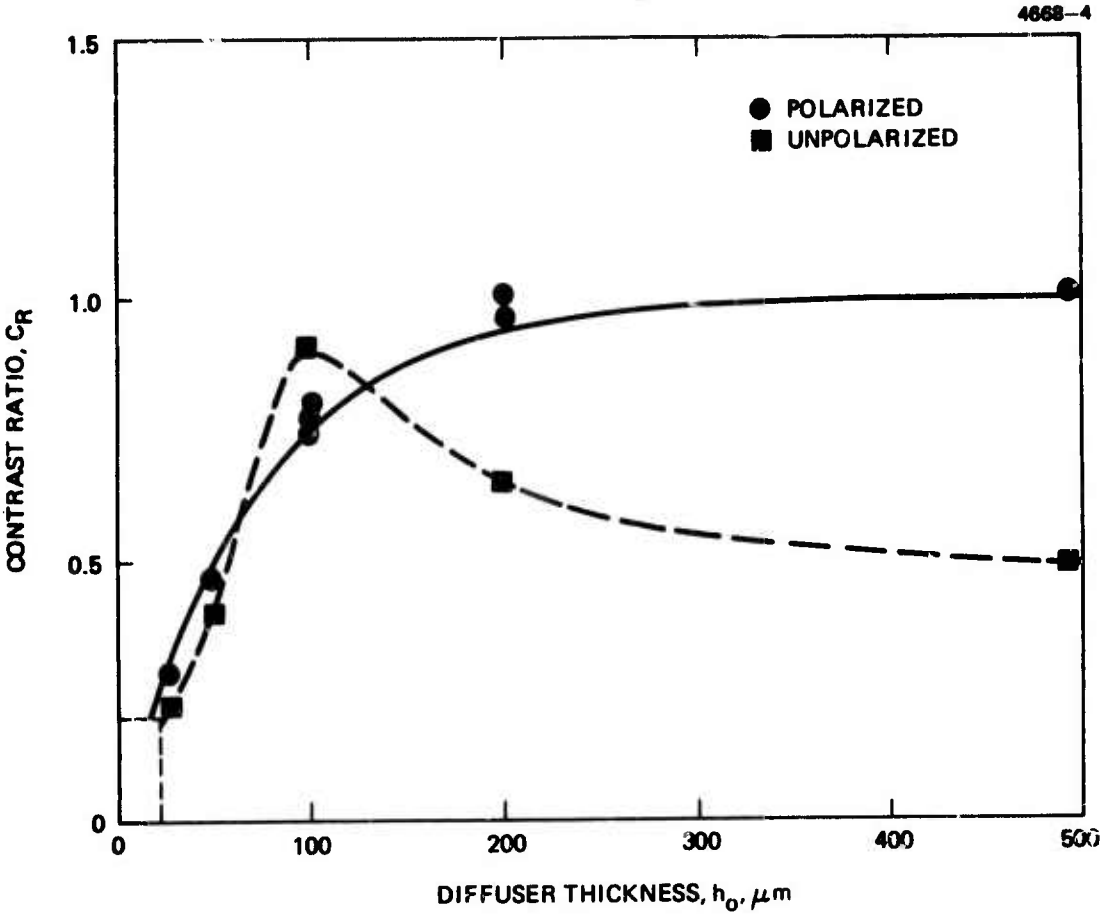

Figure 6. Contrast ratio C_R versus diffuser thickness for the opal glass diffuser series.

III. TECHNICAL ACCOMPLISHMENTS

A. Experimental Target Reflection Speckle Measurements

1. Preliminary Experimental Results

During the latter portion of the previous program entitled, "COAT Measurements and Analysis" (RADC F30602-75-C-0001), some preliminary experimental speckle measurements were made, motivated by the work of Ogrodnik and Gurski.[4] This work is reported in Quarterly Technical Report No. 3 for the period of 1 January 1975 to 31 March 1975. The relevant results obtained in that study were that a rotating scotchlite target produced a significant increase in COAT receiver speckle noise but no significant degradation in converged power, and that an artificially simulated swept narrow band speckle noise spectrum could partially degrade COAT system convergence.

2. Quasi Static Speckle Measurements

An apparatus shown in Fig. 7 was assembled to measure the speckle characteristics of various targets developed for this program. A helium neon laser beam was spatially filtered, truncated, and recollimated to 0.15 mm diameter (i.e., intensity) to simulate the converged output of the COAT system. This beam then illuminated a variety of targets at a range of 1.8 m where the beam radius was 10 mm to the first null. The targets were mounted on a motor-driven tunntable and the photomultiplier detector on a motor driven translating stage. The photomultiplier (PMT) output was processed in a lock-in amplifier and recorded via a strip chart recorder. A 100 Hz synchronous chopper placed in the path of the transmitted laser beam provided the optical modulation and the reference signal for the synchronous detector. In the series of experiments performed, either the target was rotated and the PMT was fixed, or the PMT was translated and the target was held fixed. Another parameter that was varied during the experiment was the size of the receiving aperture. Pinholes of either 0.05 mm or 0.15 mm were placed in front of the PMT for this

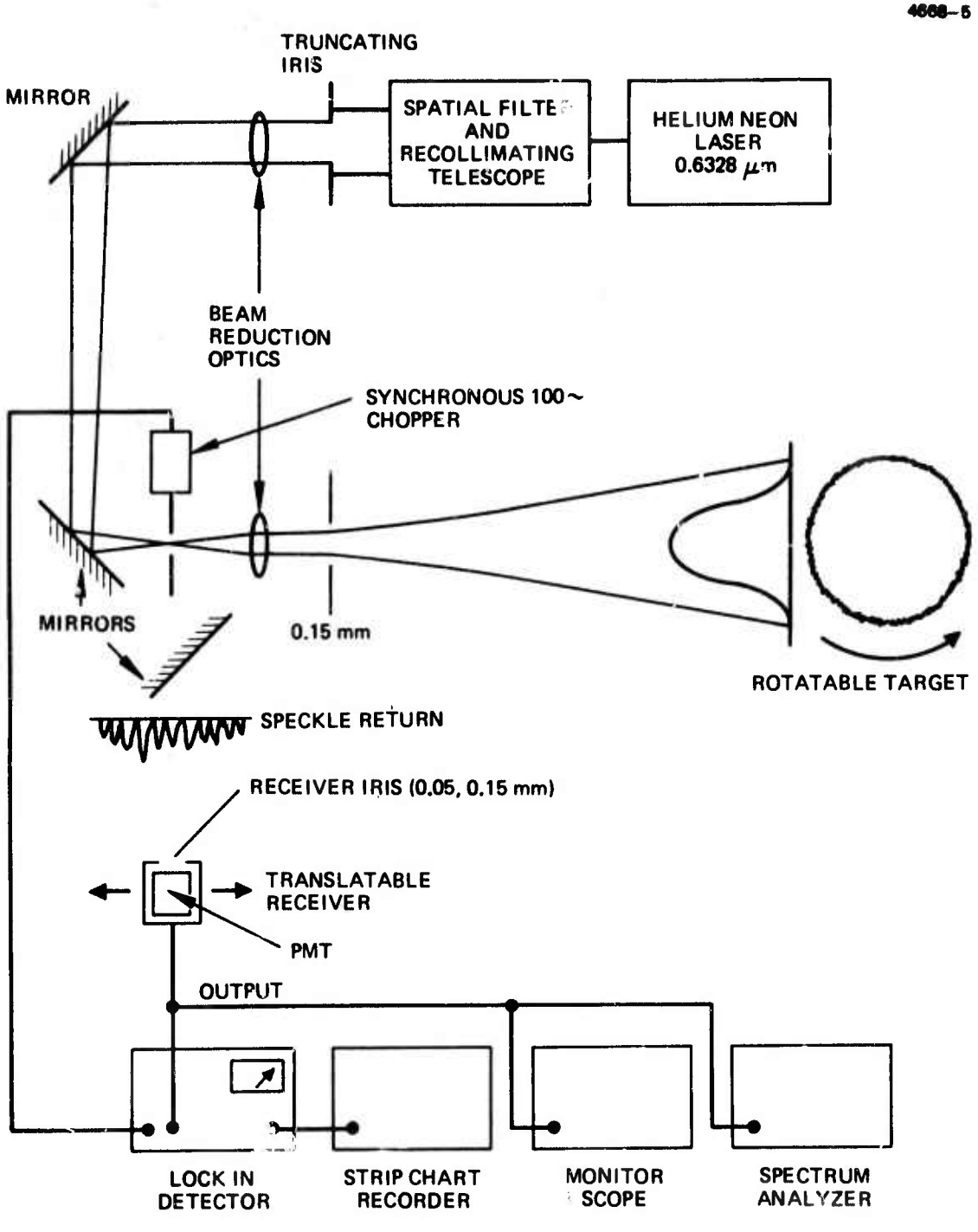

Figure 7. Schematic diagram of target speckle measurement apparatus

purpose. The larger diameter pinhole corresponded to the identical transmitter and receiver aperture diameter. Data taken with the smaller aperture showed the presence of higher spatial frequency speckle modulations which are integrated out by the larger receiver aperture. The PMT receiver was also provided with a removable polarizer to facilitate measurements of speckle contrast as a function of polarization.

Measurements were made on target spheres, cylinders, and cones fabricated from ordinary glass. Some of these targets were sandblasted, and others were left smooth. All were electroplated with nickel. Some of these targets were then coated with 3M NEXTEL white paint which shows excellent Lambertian scattering properties.

a. Spatial (Speckle) Modulation Generated by Target Rotation – The spatial modulations or optical intensity patterns produced by slowly rotating metallic spheres and cylinders are shown in Figs. 8, 9, and 10. The data in the upper curve of each figure was taken with a 0.15 mm pinhole aperture receiver and in the lower curve with a 0.05 mm aperture. Aperture-averaging with the larger receiver is clearly evidenced by the loss of high frequency information. The data taken with the smaller receiver (0.05 mm) shows higher spatial frequency content and a higher contrast ratio than that taken with the larger receiver (0.15 mm).

The maximum contrast ratios for the smooth sphere, the sandblasted sphere and the smooth cylinder obtained with the larger aperture were 0.79, 0.75, and 0.64, respectively, and 0.77, 0.89 and 0.80 when measured with the smaller aperture. The average contrast ratios were 0.73 and 0.82 for the large and small aperture. These contrast ratios were calculated by taking the maximum irradiance and an adjacent minimum and finding the ratio of the difference to the sum. The average contrast ratios observed were considerably lower. Maximum contrast ratios of 1.0 corresponding to zero nulls were not observed, possibly because of the finite receiver size. In our experiments, decreasing the aperture size increased the contrast ratio; therefore, as the aperture becomes small compared with the speckle size, the maximum observed contrast may approach 1.

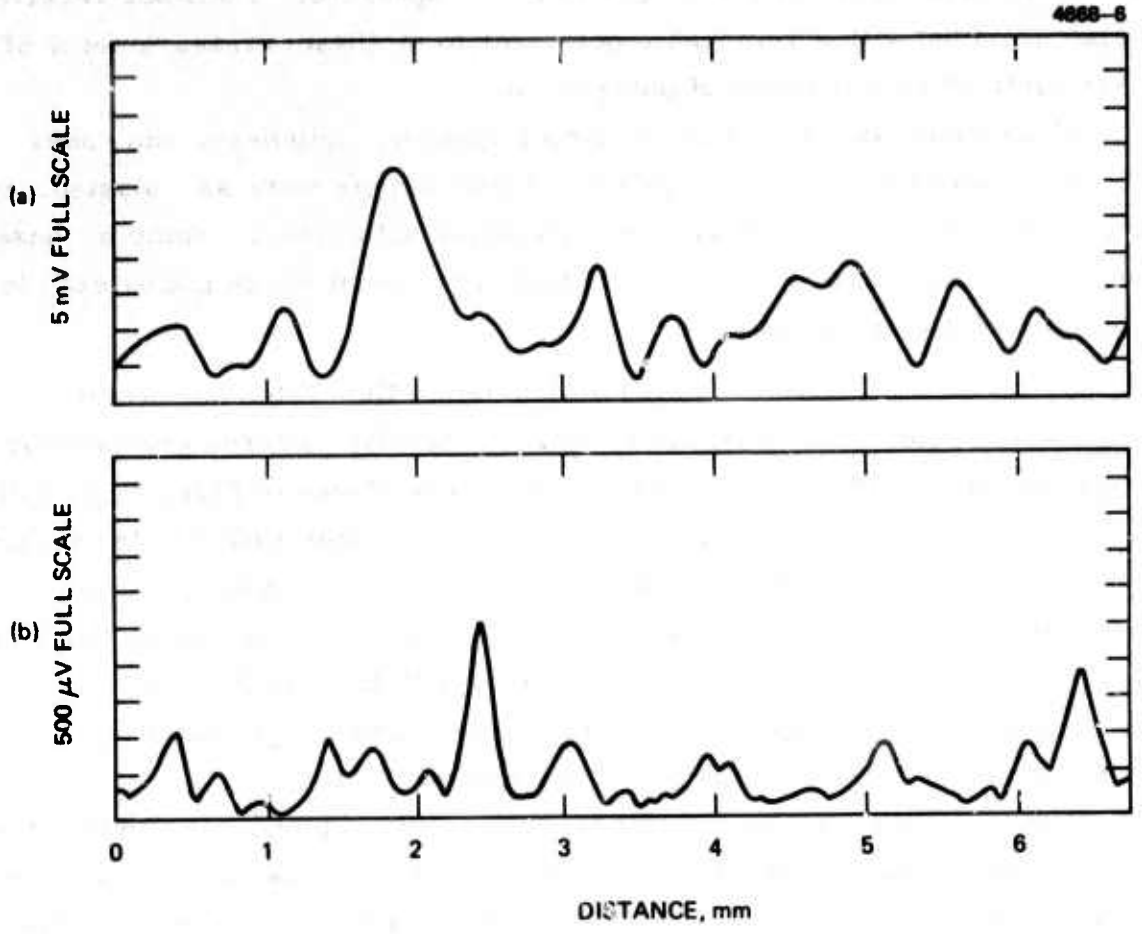

Figure 8. Speckle patterns generated by rotation of a smooth metallized sphere.
(a) 0.15 mm receiver
(b) 0.05 mm receiver

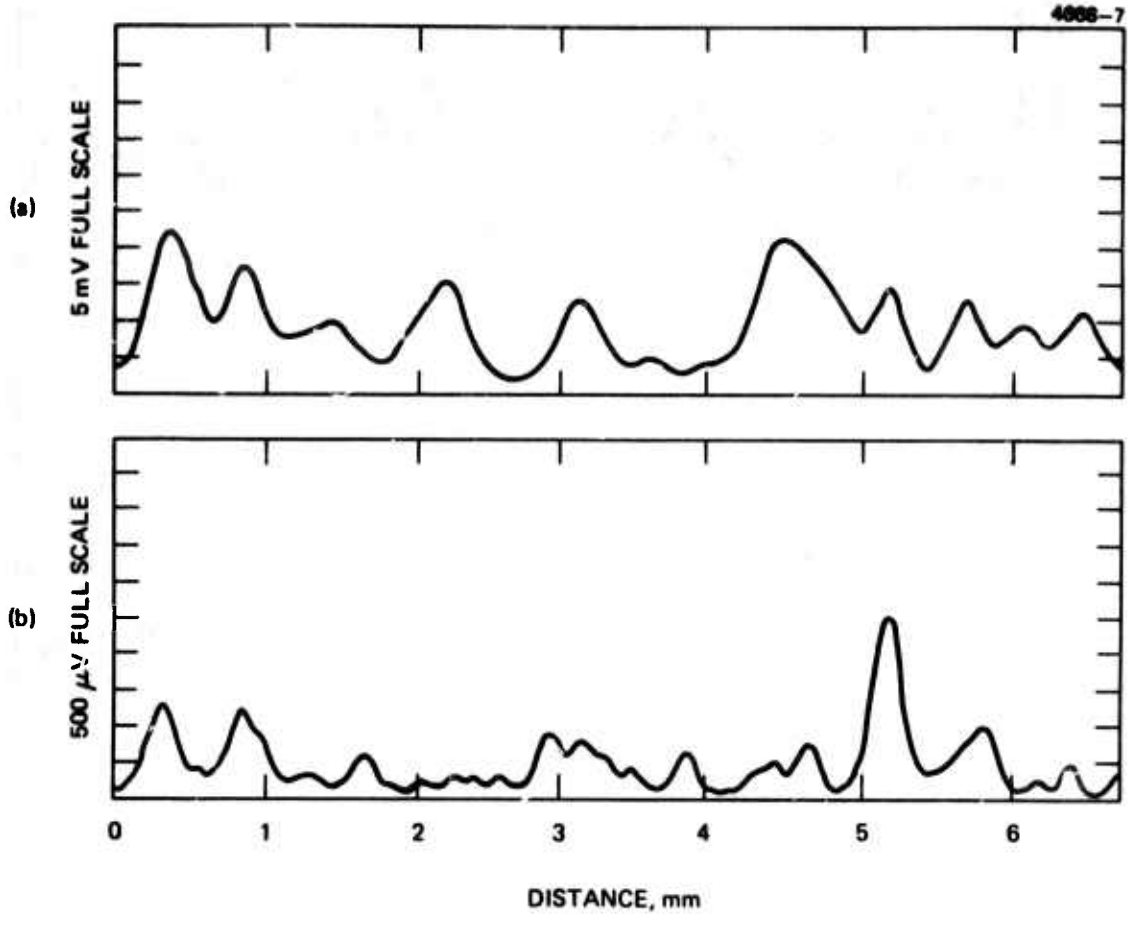

Figure 9. Speckle patterns generated by rotation of rough metallized sphere.
(a) 0.15 mm receiver
(b) 0.05 mm receiver

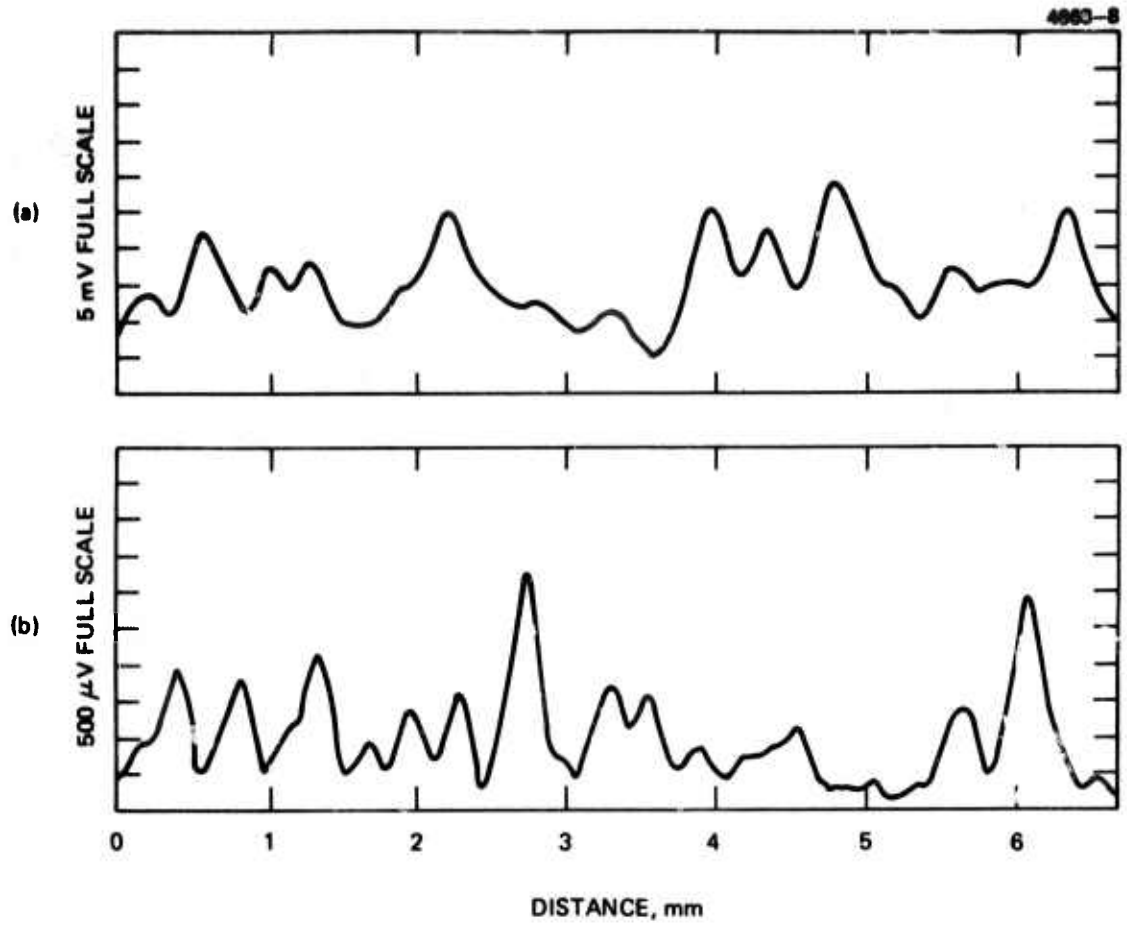

Figure 10. Smooth metallized sphere speckle patterns generated by rotation
(a) 0.15 mm receiver
(b) 0.05 mm receiver

After a careful study of these data, we conclude that the shape of the target and the nature of the surface roughness does not significantly affect the spatial modulation spectrum or the average contrast ratio, as long as the entire illuminating beam is smaller than the target.

b. Equivalence of Rotational and Translational Speckle Modulations and Spatial Frequency Spectra — It was necessary to measure the relationship between rotationally and translationally generated speckle modulations to simplify the number of COAT convergence experiments required in the next phase of the program. The translation experiment is

particularly troublesome, since it cannot be performed continuously at constant velocity and since it requir s twice as many measurements as the rotational experiment.

We have measured speckle signatures independently by detector translation and by target rotation. These two measurements are not equivalent because rotation of the target through a small angle produces a small change in the scattering surface near the periphery of the beam. As long as the rotation angles are small, however, this is a small effect. Several data records, in fact, exhibited speckle patterns that were almost mirror images of each other when the translation-rotation functions are appropriately sequenced. Figure 11 shows an example of this type of data. This result establishes that for small angles of rotation or for small translations two motions were equivalent.

3. Spatial Frequency Analysis

The spatial frequency spectrum of the speckle data for the smooth sphere shown in Fig. 8 has been calculated via a fast Fourier transform (FFT) routine. Figure 12(a) represents the speckle spectrum of a

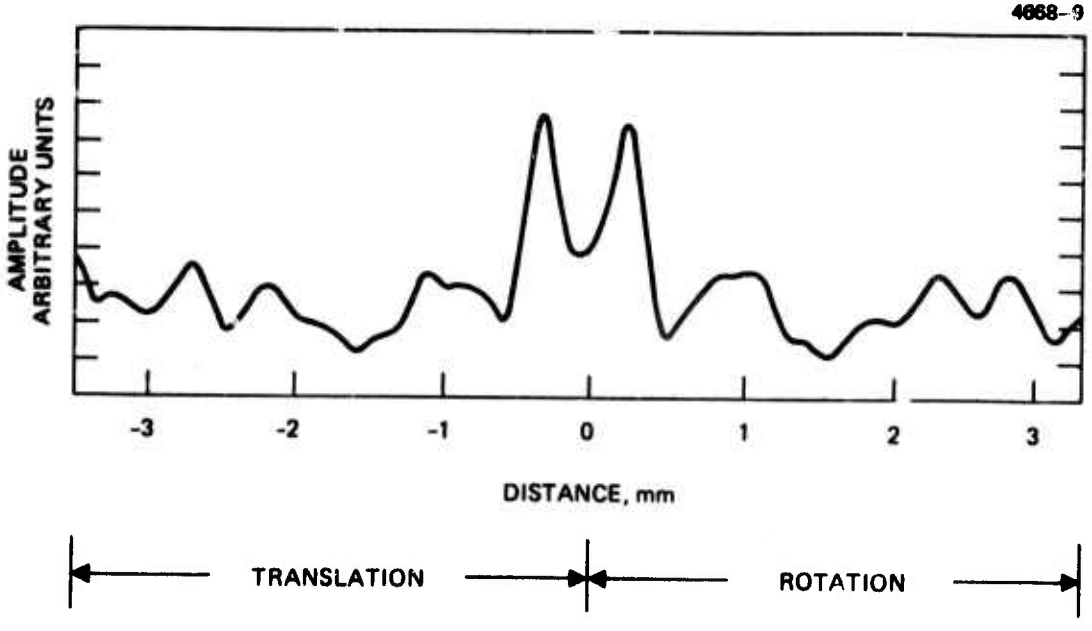

Figure 11. Symmetry of rotational and translational speckle modulation patterns.

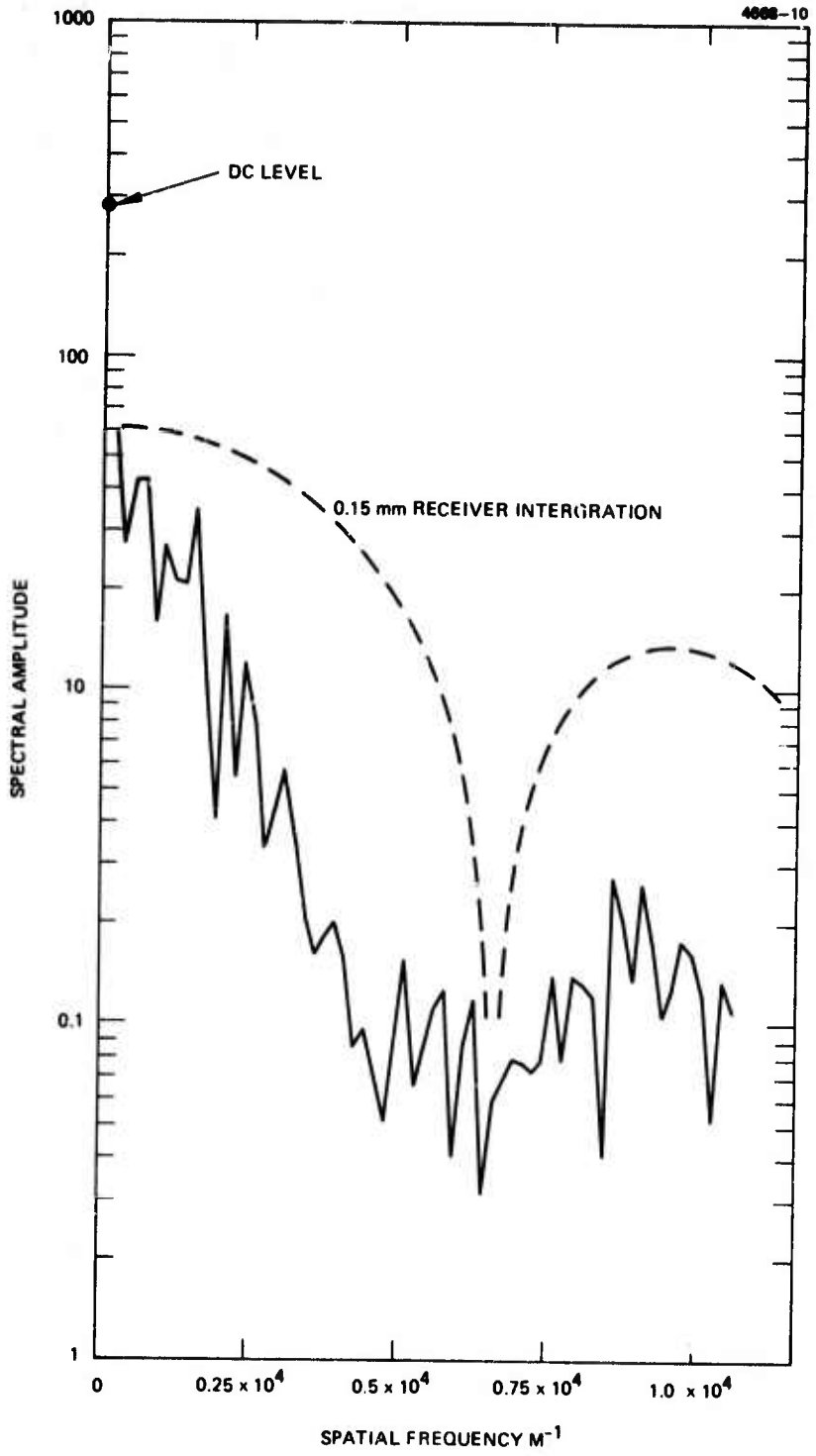

Figure 12(a). Spatial frequency spectrum of smooth metallized sphere — 0.15 mm receiver.

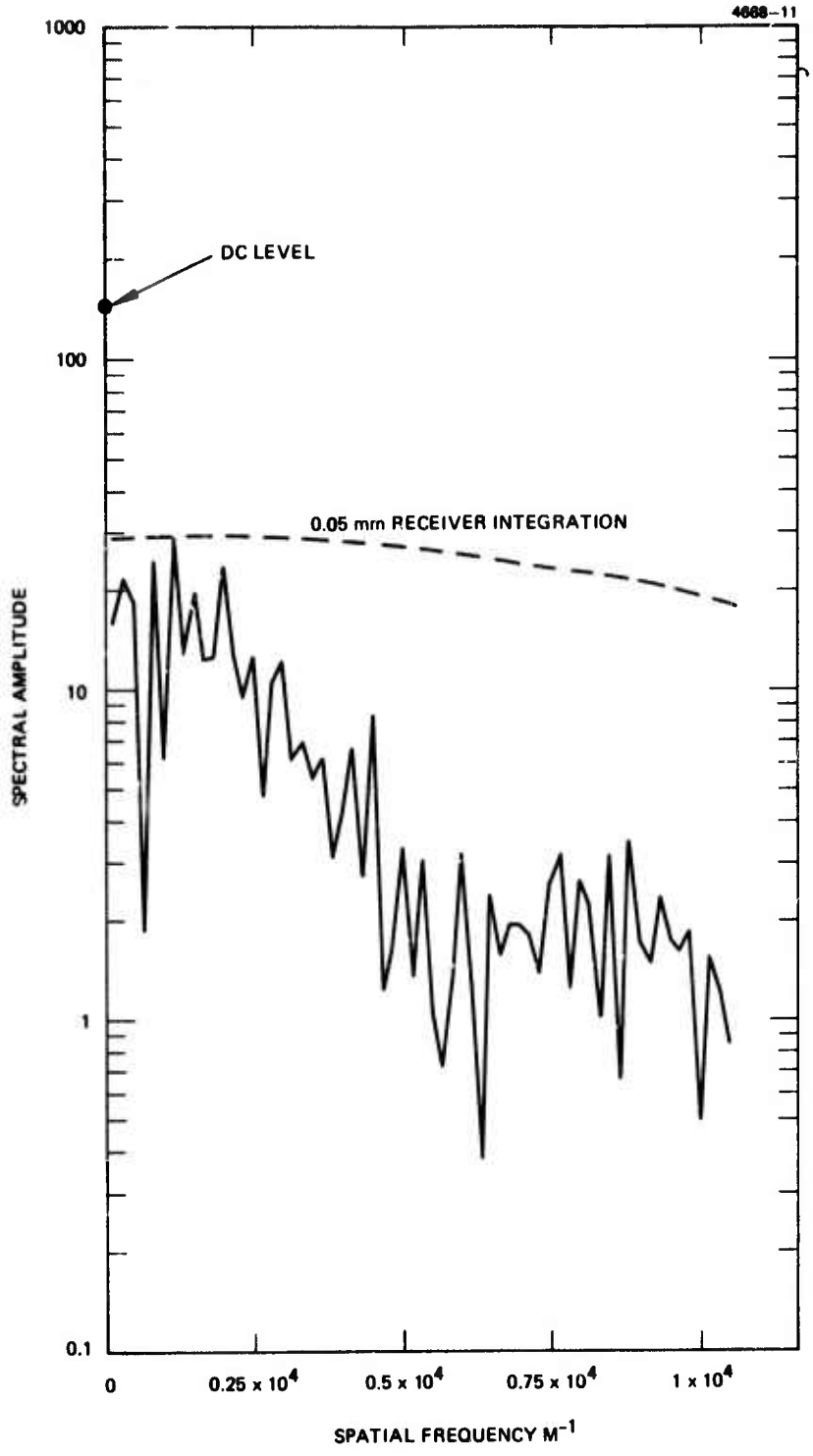

Figure 12(b). Spatial frequency spectrum of smooth metallized sphere — 0.05 mm receiver.

rotating target seen by a 0.15 mm receiver. When the receiver is translated, the general shape of the spectrum is very similar to that shown in Fig. 12(b). The notch in the spectrum centered about $0.67 \times 10^{4} M^{-1}$ is attributed to the spatial integration of the signature by the finite aperture. Figure 12(b) represents the same spectrum received by a 0.05 mm receiver. Notice the improvement of the higher frequency components relative to the lows. A naive approach to the effect of finite aperture integration eliminates all spatial frequencies higher than that corresponding to the receiver aperture. The calculated data for a one dimensional slit of 0.15 mm width shown in Fig. 12(a) clearly shows the presence of higher spatial frequencies at a level 13 dB below the maximum. Figure 12(b) shows the effect of aperture integration with a receiver one third the size of the transmitter (0.05 mm). The relative effect of aperture integration is that the larger aperture reduces the high frequency spectrum relative to the low by 9 dB.

The absolute effect of aperture integration by the larger aperture relative to a point receiver is to reduce the target signature spectrum by 11 to 13 dB for all frequencies beyond the aperture cutoff frequency. Also, all frequencies greater than one-half the large aperture cutoff frequency are attenuated by more than 3 dB. These results substantiate our experimental findings in Figs. 8, 9, and 10 of lowered speckle signature contrast when integration by the larger aperture is present.

Signatures of sandblasted metallized spheres with an integrating aperture of 0.15 mm are very similar to the smooth sphere case. The spectrum for this case is shown in Fig. 13 and is very similar to those analyzed for the smooth sphere. This result shows that the nature of the speckle spectrum is primarily determined by the target illumination function and the surface shape, and not by the state of the surface for this class of specular metallized targets.

Figures 14(a) and (b) show the speckle target signatures obtained by rotating a smooth metallized cone about an axis parallel to the base of the cone. This signnature is the anomally of the data taken in this program. The low apparent periodicity is partially explained by the geometry of the conical surface. The only significant backscatter appears to be generated at the nose of the cone. This implies that the effective dimension of the

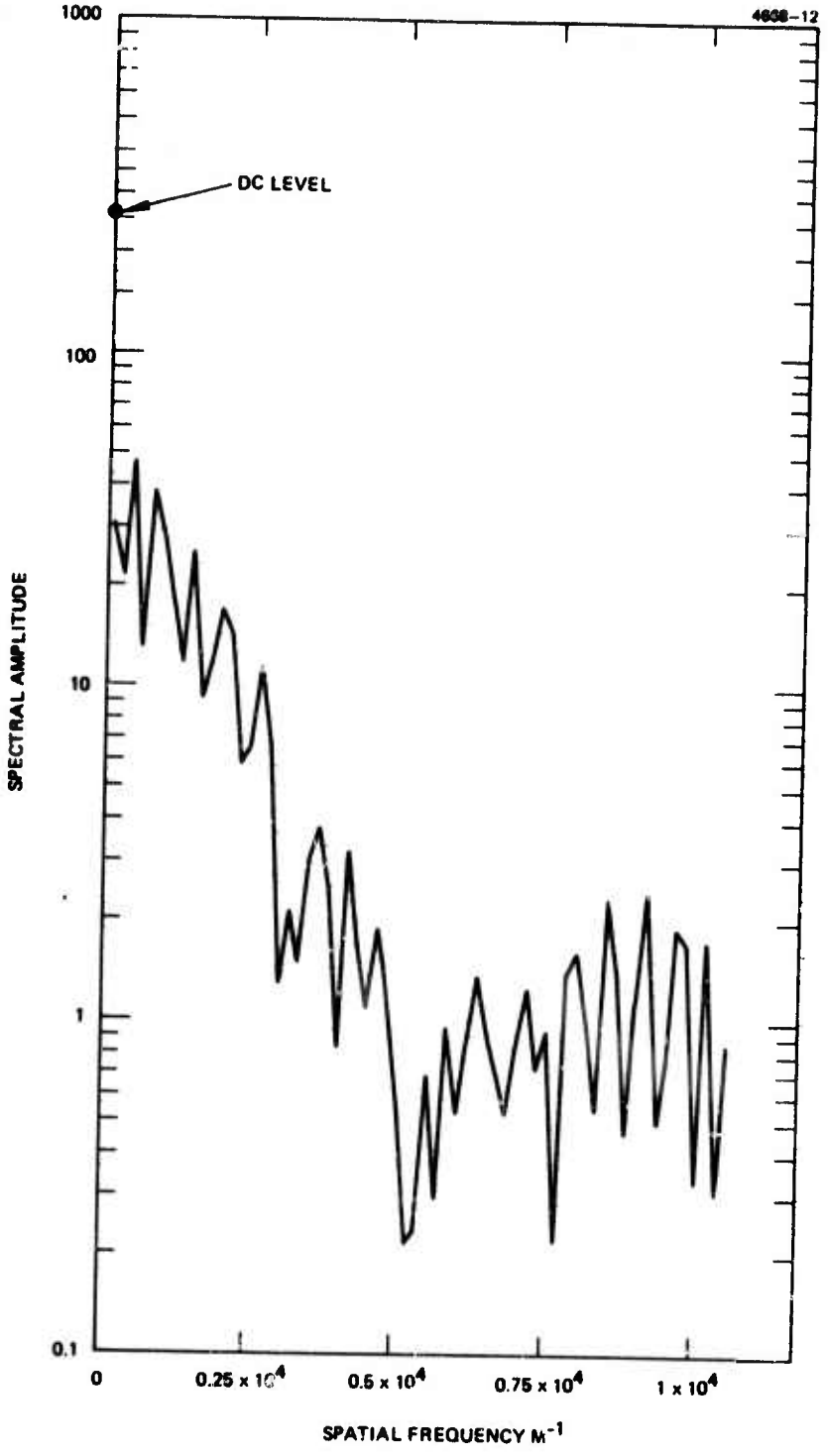

Figure 13. Spatial frequency spectrum of speckle from rough metallized sphere (0.15 mm receiver).

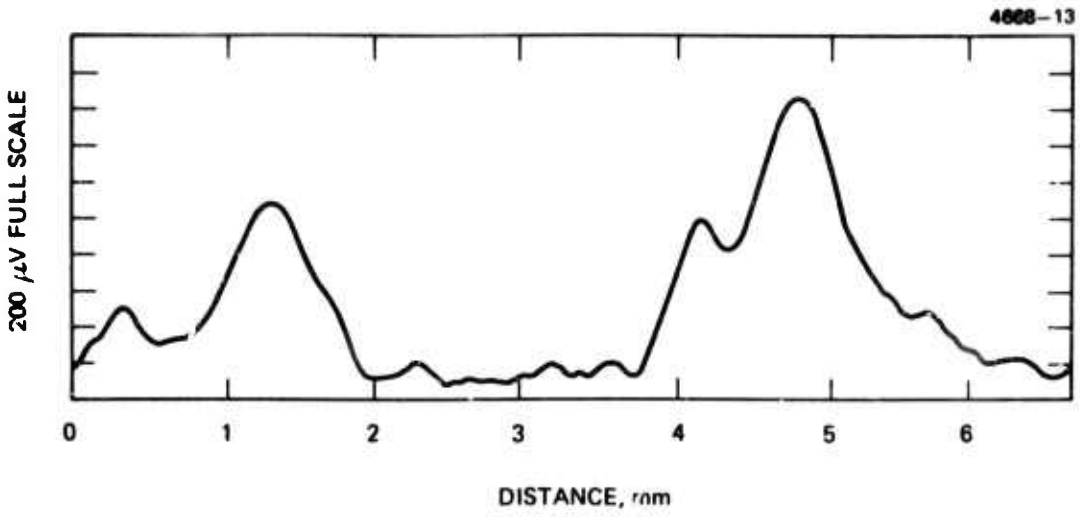

Figure 14. Speckle pattern from smooth metallized cone with axial illumination.

speckle generator is smaller than the illumination function, and that the speckle spatial period should be large. However, the speckle pattern is not sinusoidal but highly triangular and therefore rich in spatial frequency harmonics. The FFT spectrum is shown in Fig. 15. This spectrum drops from the dc level by approximately 16 dB at high frequencies. The aperiodic nature of the spatial function explains presence of high frequencies in the spectrum. The linear slope of the spectrum plotted on log paper corresponds to an exponential or Gaussian frequency distribution. Thus, the observed spatial frequency spectrum is qualitatively in agreement with the theory (see Section II-A, eqs. 10 to 13).

Target velocity and rotation rate govern the real time frequency spectrum generated in a receiver by speckle modulation. The real time spectrum $G(f_t)$ can be found from the spatial frequency spectrum $G(F_x)$ by the relationships

$$f_t = (F_x) \cdot (V_x)$$

or

$$f_t = (F_x) \cdot (2\Omega_x) \cdot Z \quad ,$$

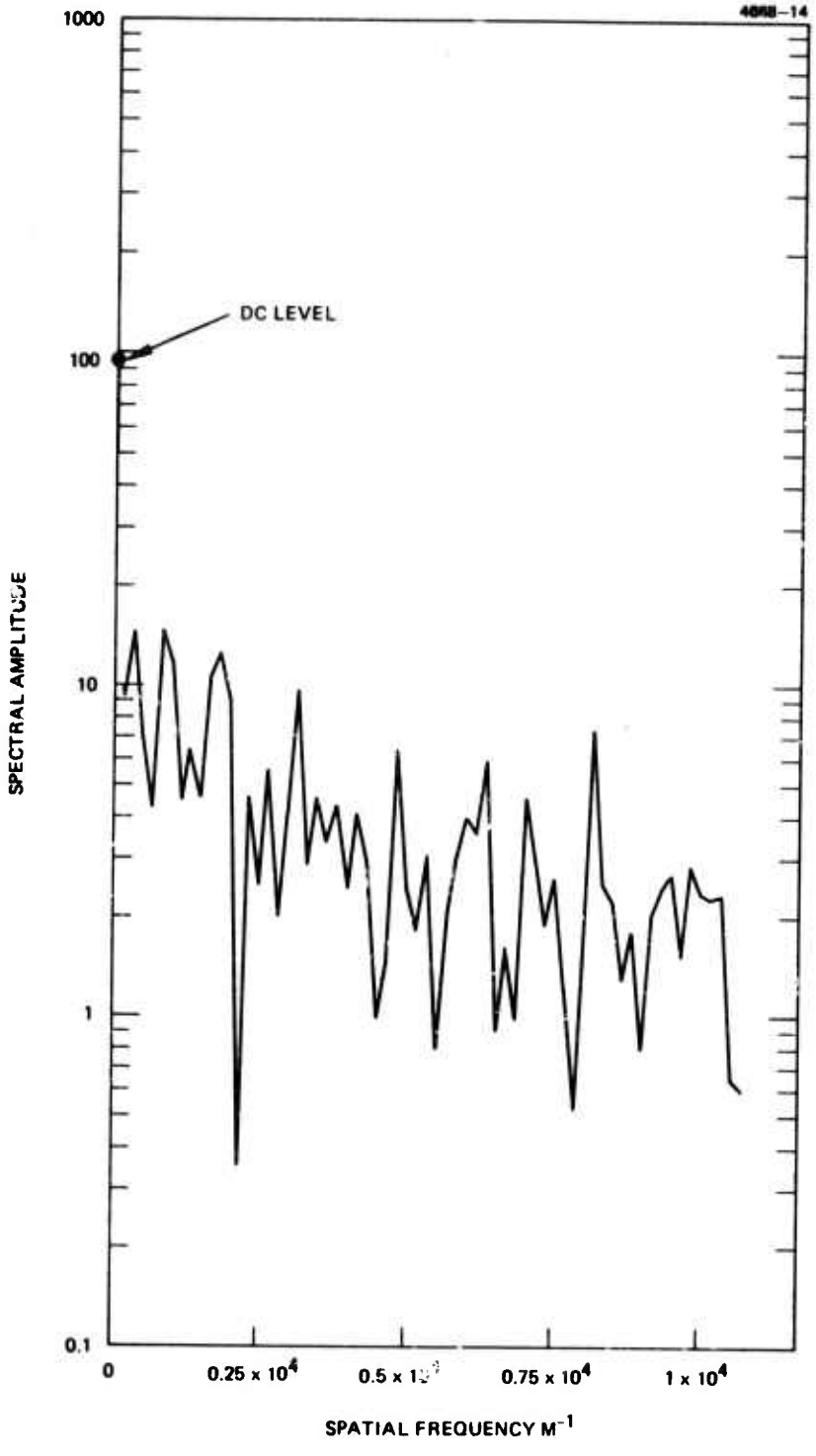

Figure 15. Spatial frequency spectrum of endwise illuminated smooth metallized cone.

where V_x is the relative velocity of the receiver and the target, Ω_x is the relative angular velocity of the target, Z is the target to receiver distance, f_t is the temporal frequency (sec^{-1}) and F_x is the speckle spatial frequency (m^{-1}).

The pertinent parameters for our scaled laboratory version of a typical target scenario are shown in Table 1. As an example, at the experimental spatial frequency midband ($F_C = 0.5 \times 10^4\ m^{-1}$), the temporal frequencies f_t are 4 kHz and 540 Hz for translation and rotation, respectively.

Table 1. Parameters Determining Speckle Modulation Spectrum

Parameters	Real Scenario	Scaled Laboratory Model
Wavelength	$\lambda = 3.8\ \mu m$	$\lambda = 0.6328\ \mu m$
Range	$Z = 4 \times 10^3$ m	$z = 1.8$ m
Transmitter Aperture	$D_T = 0.7$ m	$d_t = 0.15 \times 10^{-3}$ m
Target Translation Velocity	$V_s = 4 \times 10^3$ m/sec	$v_s = V_s D_t / D_T$ $= 8 \times 10^{-1}$ m/sec
Target Angular Velocity	$\Omega_x = 0.06$ rad/sec	$\omega_x = \left(ZD_t / zD_T\right) \cdot \Omega_x$ $= 0.03$ rad/sec

4. Target Surface Phenomena

Figure 16 compares the speckle modulation signatures generated by rotating a smooth metallized sphere and a white painted sphere. The integrating aperture size for these data and for the remainder of this section is 0.15 mm. The maximum speckle contrast ratios for the smooth metallized sphere and the white sphere were found to be 0.79 and 0.42, respectively. The Lambertian scattering characteristics of the white surface (known from measurements on other programs) was expected to produce less

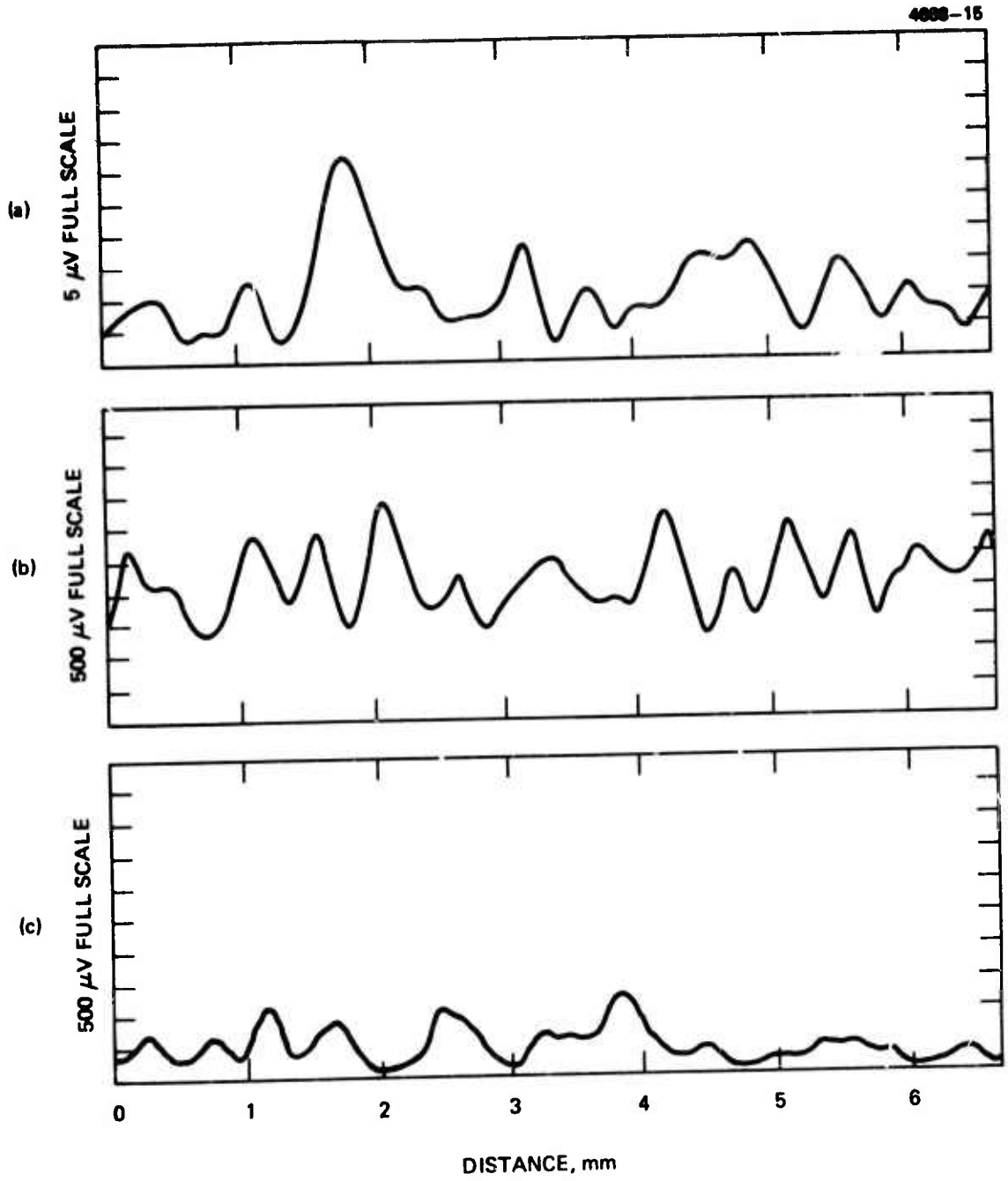

Figure 16. Speckle patterns of rotated sphere
(a) Smooth sphere – 0.15 mm receiver
(b) White sphere – 0.15 mm receiver
(c) White sphere – 0.15 mm receiver polarized

specular scattering and a higher contrast ratio. However, approximately half of the scattered energy is depolarized and the speckle pattern for the orthogonal polarization is uncorrelated with that of the incident polarization. Figure 16(c) shows the effect of placing a polarizer in front of the detector oriented parallel to the transmitted polarization. The maximum contrast ratio increased to 0.71. This result qualitatively substantiates the theory and allows us to predict that with true Lambertian scatterers, the speckle contrast ratio will be substantially less than 0.71, provided the receiver is not polarized and aperture averaging is employed.

One of the more interesting target shapes studied has been the cone. The results of a series of measurements on a cone illuminated from the side are shown in Fig. 17. In the case of the smooth metallized cone (Fig. 17(a)), the low maximum contrast ratio of 0.17 was attributed to the specular nature of the cone reflectance. The rougher metallized cone surface data shown in Fig. 17(b) showed a higher contrast ratio of 0.43. A contrast ratio of 0.58 was generated by the white cone data shown in Fig. 17(c).

A similar set of experimental results is presented in Fig. 18 for a cone-shaped target illuminated head-on. As mentioned before, the anomalously low periodicity in Fig. 18(a) is explained by the small nose cross section. The maximum contrast ratio of 0.79 is consistent with a reflector which produces very little specular scattering in the direction of the receiver because of its geometrical shape. The rough cone result in Fig. 18(b) shows higher spatial frequency content and lower contrast ratio of 0.56. In Fig. 18(c), the white cone shows similar spatial frequency content to the rough cone of Fig. 18(b), except that the maximum contrast ratio of 0.35 is significantly lower. The mechanism of Lambertian depolarization of the target return at normal incidence can explain this contrast reduction; when these targets are illuminated with the laser and observed through a polarizer only slight depolarization is seen for the metallized surfaces, but total depolarization is observed for the white surfaces.

A tabulation of all of the measured maximum contrast ratios is given in Table 2. The largest contrast observed with equal transmitter and receiver apertures was 0.79 and the average of the maximum was 0.56. The average speckle contrast ratio observed in any experiment was of the order of 0.5 or less.

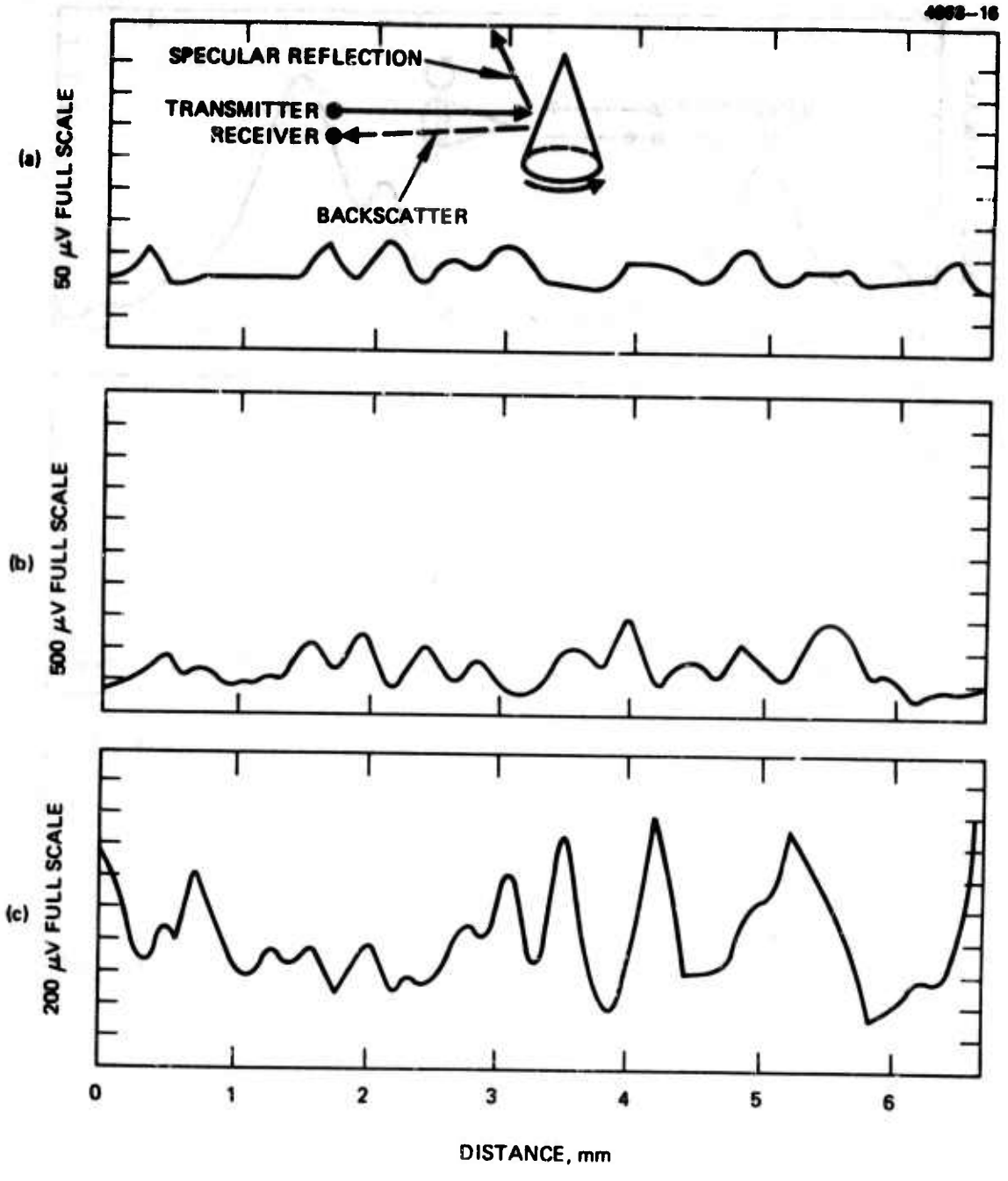

Figure 17. Speckle patterns of cones with side illumination and 0.15 m receiver size
(a) Smooth metallized cone
(b) Rough metallized cone
(c) White painted cone

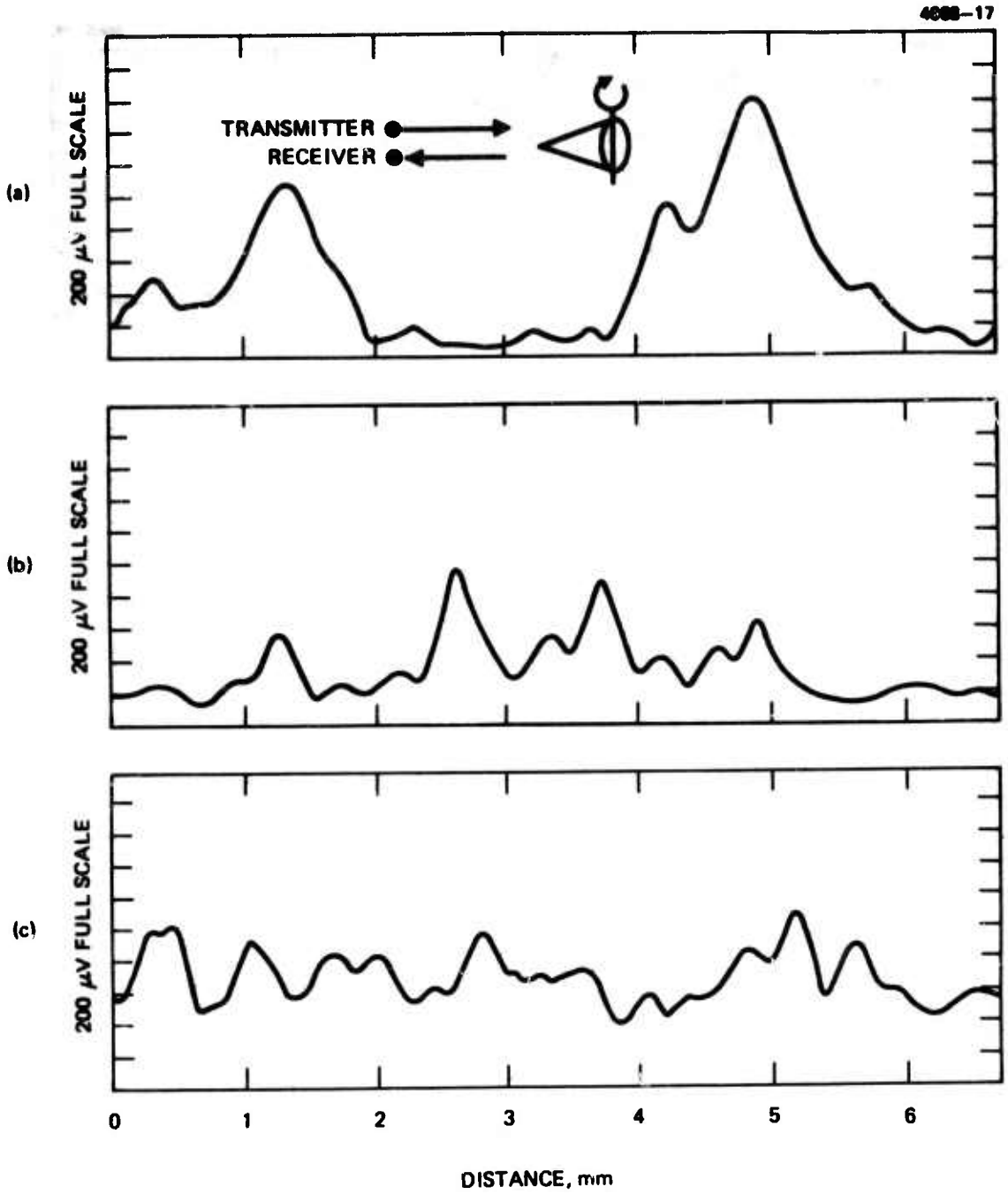

Figure 18. Speckle patterns of cones with axial illumination and nonaxial rotation
(a) Smooth metallized cone, 0.15 mm aperture
(b) Rough metallized cone, 0.15 mm aperture
(c) White painted cone, 0.15 mm aperture

5. Dynamic Speckle Measurements

The real time amplitude spectral density of some of the realistic target models described in the previous section were measured by rotating the targets at various speeds. The receiver signal was then observed with a spectrum analyzer (see Fig. 7). The spectra observed generally agreed with the preliminary experimental results obtained on the previous

Table 2. Maximum Speckle Contrast Ratios of Variously Shaped and Surfaced Targets

Target	Maximum Contrast Ratio	
	Aperture, 0.15 mm	Aperture, 0.05 mm
Smooth Sphere	0.79	0.77
Rough Sphere	0.75	0.89
Smooth Cylinder	0.64	0.80
Average	0.73	0.82
Smooth Sphere	0.79	
White Sphere	0.42	
White Sphere (Polarized)	0.71	
Smooth Cone (Side) Illumination	0.17	
Rough Cone (Side) Illumination	0.43	
White Cone (Side) Illumination	0.58	
Smooth Cone (End) Illumination	0.79	
Rough Cone (End) Illumination	0.56	
White Cone (End) Illumination	0.35	
Average	0.56	

contract[5] with a rotating scotchlite cylinder, and with the detailed spatial frequency spectra extracted from the realistic target speckle signature data.

Figure 19 shows the spectrum of a smooth metallized spherical target in a stationary condition and rotated at 0.67 revolutions per second, the data having been taken at 10 and 200 Hz bandwidth. Aside from a 0.4 gain factor for the 200 Hz bandwidth case, the spectral results are very similar. The noise spectral amplitude due to speckle is approximately a factor of 2.8 larger than the photodetector and laser noise for both cases. This result is very similar to that obtained earlier for scotchlite targets.[5]

A similar set of test results is shown in Fig. 20 for the smooth metallized cylindrical target. The cylindrical geometry tends to produce spreading of the scattered energy in only one coordinate direction as compared to the uniform angular scattering from the spherical target. This leads to a stronger speckle signal as evidenced by the speckle noise being a factor of 3.8 greater than the system noise.

The effect of varying the target rotation rate is shown in Figs. 21 and 22 for the spherical and cylindrical targets. A definite shift of the amplitude spectrum toward high frequencies with increasing target speed is evident in both cases. The larger receiver speckle signal-to-noise ratio produced by the cylinder makes the effect more pronounced. The amplitude spectral density is always larger at the low frequency end but increases at higher frequencies with increasing target rotation speed. In other words, the frequency of the 3 dB speckle noise level shifts proportionately with rotation rate. This is in exact agreement with the discrete spatial frequency spectral data analysis of the previous section, where the spatial spectrum is always stronger at low frequencies and falls off at high frequencies due to the Gaussian illumination function and due to the aperture averaging effect. Since the temporal frequency is obtained from the spatial frequency by multiplication by the product of the angular rate and the range, this spectrum is either expanded or compressed as the velocity of the target is changed, but its shape is basically unchanged. If the target is rotated fast enough, the speckle noise spectrum will appear flat because the 3 dB cutoff will fall outside

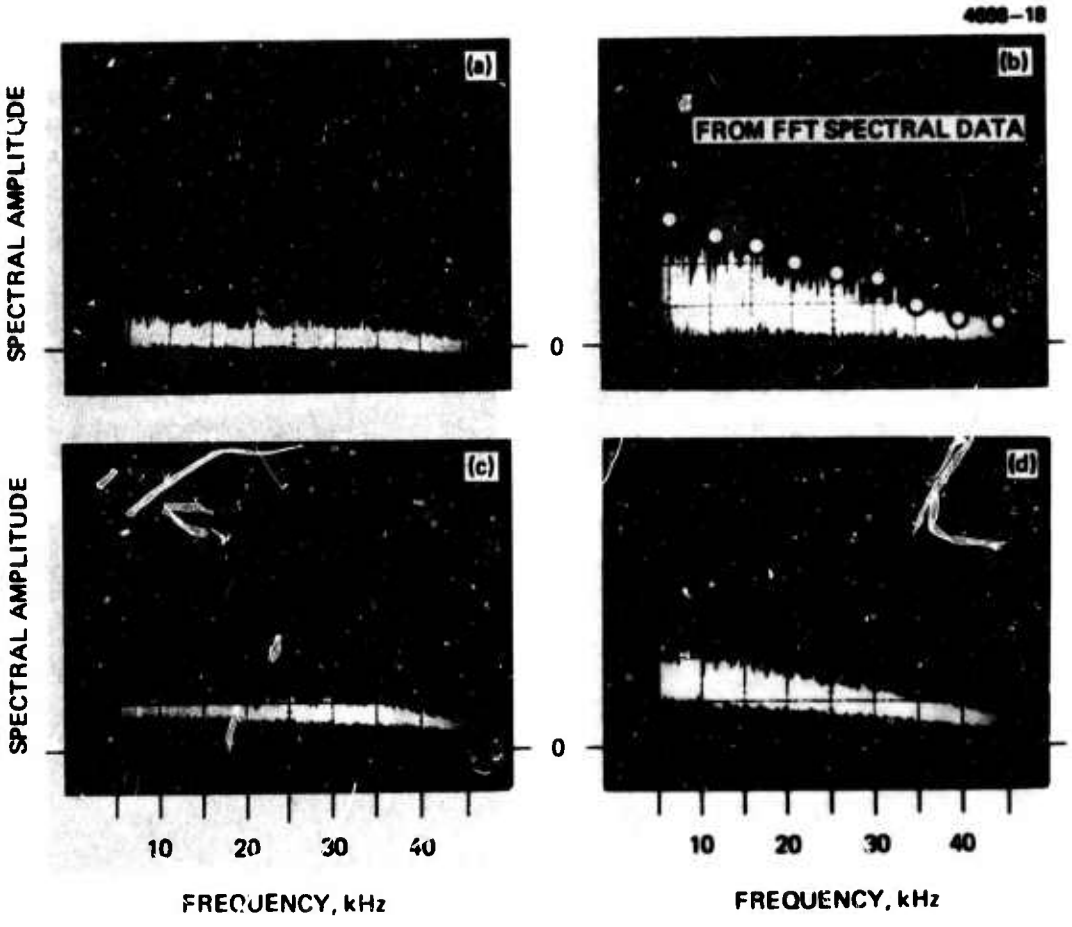

Figure 19. Receiver signal amplitude spectra for smooth spherical metallized target. (a) and (c) Stationary target, (b) and (d) Rotating target. The spectrum analyzer bandwidth is 10 Hz in (a) and (b) and is 200 Hz in (c) and (d). Target rotation rate 0.67 rps.

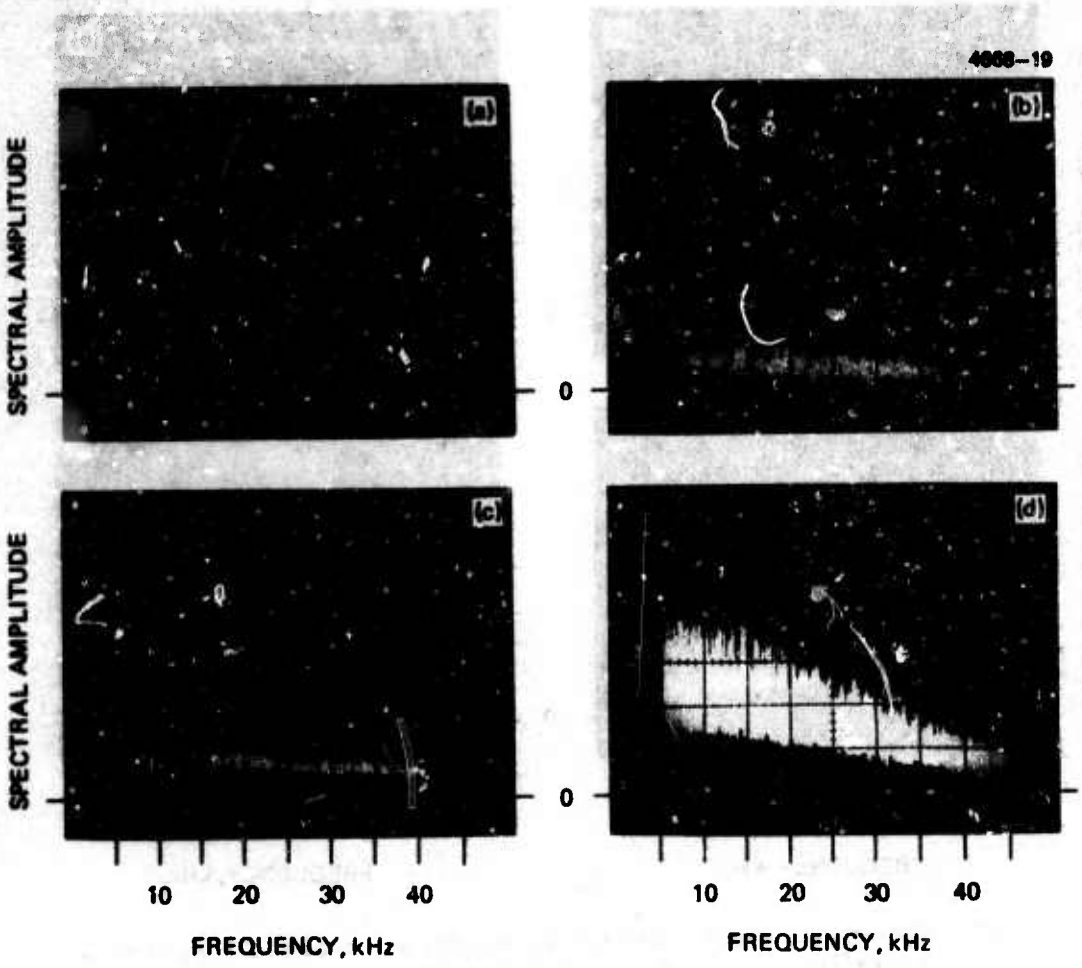

Figure 20. Receiver signal amplitude spectra for smooth cylindrical metallized target. (a) and (c) Stationary target. (b) and (d) Rotating target. The spectrum analyzer bandwidth is 10 Hz in (a) and (b) and is 200 Hz in (c) and (d). Target rotation rate is 0.67 rps.

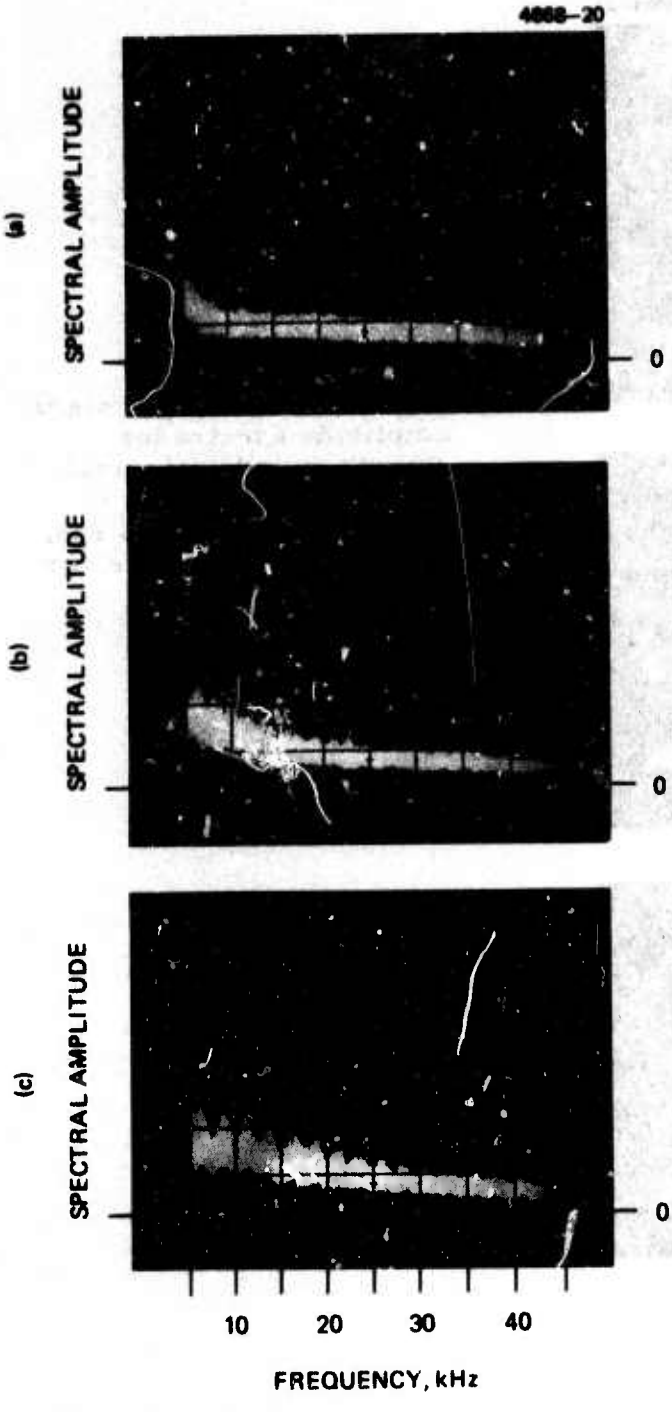

Figure 21. Receiver signal amplitude spectra for smooth spherical rotating target. The rotation rates are (a) 0.11 rps, (b) 0.25 rps, (c) 0.38 rps. The receiver bandwidth is 200 Hz.

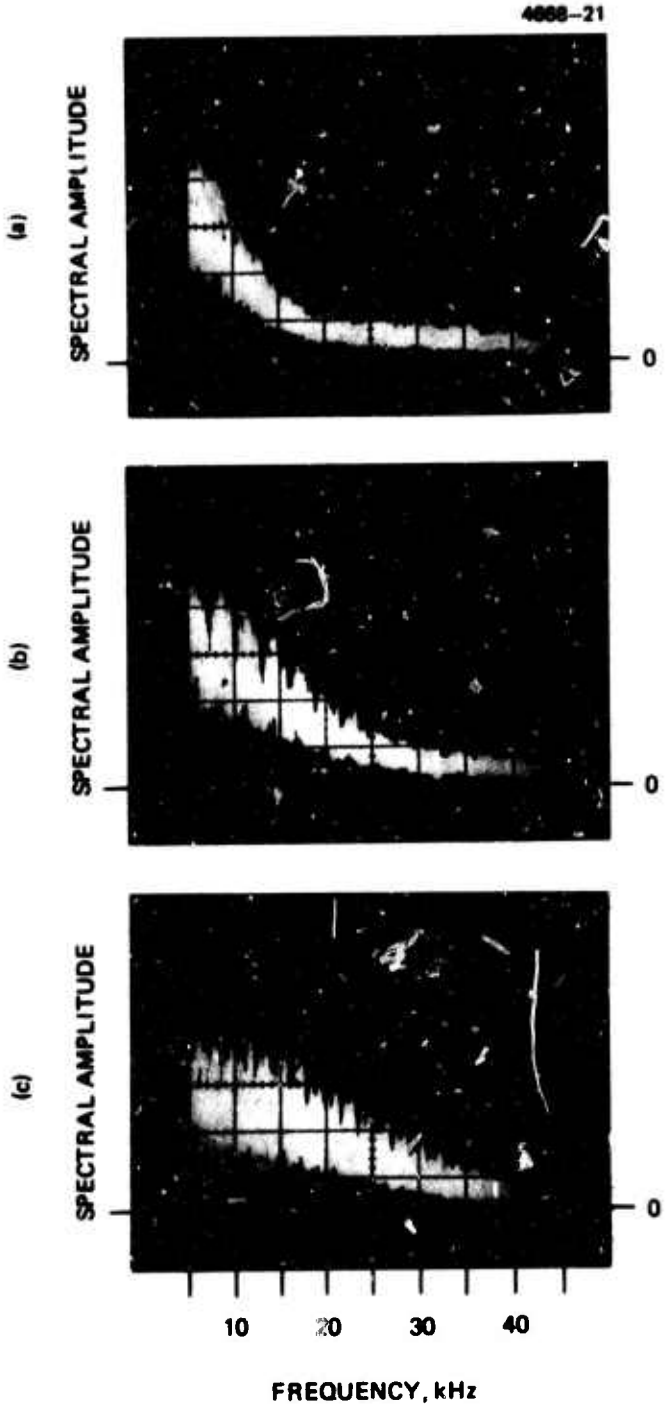

Figure 22. Receiver signal amplitude spectra for smooth cylindrical metallized rotating target. (a) 0.21 rps, (b) 0.33 rps, (c) 0.5 rps. The receiver bandwidth is 200 Hz.

the displayed spectral range. A table of speckle modulation frequencies as a function of target rotation rates is given in Table 3. A dividing line bounds the -3 dB signal amplitude regime.

Table 3. Modulation Frequency as a Function of Spatial Frequency and Rotation Rate

Rotation Rate →	0.25 RPS	0.5 RPS	0.75 RPS	1 RPS
Spatial Frequency	Modulation Frequencies, kHz			
0×10^4 M^{-1}	0	0	0	0
0.25×10^4 M^{-1}	14	28	42	57
0.50×10^4 M^{-1}	28	57	84	113
0.75×10^4 M^{-1}	42	85	127	170
1.00×10^4 M^{-1}	57	113	170	226

NOTE: (Doubleline is approximate location of -3 dB amplitude response.)

A similar set of experiments was performed with a painted spherical target, known to be a good Lambertian scatterer. This target yielded equal energy in both return polarizations and a very low speckle noise contribution when recorded with an unpolarized receiver. This result is identical to that measured in the quasi static case.

IV. SPECKLE EFFECTS ON MULTIDITHER SYSTEMS

A. Analytical Model of Speckle Modulation

The statistical analysis reported earlier has been generalized to be applicable to any generalized speckle modulation function, M_s. Originally, the whole analysis was based on a speckle modulation function with a randomly chosen, discrete frequency spectrum centered around each dither frequency over a very narrow bandwidth. The amplitude of this modulation was characterized by a parameter a_{max}, and COAT system convergence levels were predicted as a function of a_{max}. This made the analytical data very easy to compare to computer simulation data. With a more general type of modulation, however, the parameter a_{max} may be difficult or perhaps impossible to define. Thus, we consider the very general type of speckle modulation function defined by

$$M_s(t) \equiv \frac{1}{\sqrt{2\pi}} \int_{-\infty}^{\infty} d\omega \, a(\omega) \, e^{-i\omega t} \quad . \tag{14}$$

The Fourier transform relationship is

$$a(\omega) = \frac{1}{\sqrt{2\pi}} \int_{-\infty}^{\infty} dt \, M_s(t) \, e^{i\omega t} \quad . \tag{15}$$

To be physically meaningful $M_s(t)$ must always be nonnegative. Negative values imply negative intensity at the receiver, which is obviously nonphysical. Conservation of energy also requires that the average value of $M_s(t)$ be unity. We illustrate this point as follows. In the computer simulations of the COAT servo (see next section), we do not include the effect of atmospheric propagation. The receiver signal is therefore just a constant multiplied by the instantaneous intensity of the light on the target glint. The instantaneous energy incident on the receiver is thus directly proportional to

the energy incident on the glint. When speckle effects are introduced into the simulation and into the statistical analysis, we simply multiply the receiver signal by a modulation function, $M_s(t)$. Since speckle is a wave – interference effect, as opposed to an absorption or scattering effect, it must be unrelated to the total energy in the incident or reflected fields. In other words, since speckle is an energy conserving phenomena, it must be introduced in such a way that the total energy in the reflected field is unaltered. This is accomplished in the computer simulations and in the statistical analysis by requiring that the average energy incident on the receiver remain the same with or without the modulation function $M_s(t)$. The intensity at the receiver is no longer required to be instantaneously proportional to the intensity on the target glint but the average intensity at the receiver must be proportional to the average intensity on the glint, and the constant of proportionality, K, must still be the same. Mathematically this implies that the mean value or dc level of $M_s(t)$ must be unity.

Since we are interested in the power ratio of the COAT system dither signal to the speckle induced signal, we first calculate the average power flux at the receiver due to speckle modulations alone. (i.e. We assume the usual "no-speckle" intensity is unity). While the total dc level must be unity, as discussed above, the ac power at the dither frequencies is yet to be determined. By definition, the total average power in the speckle modulation, P_{TS}, is:

$$P_{TS} = \lim_{T\to\infty} \frac{1}{2T} \int_{-T}^{T} M_s(t)\, M_s(t)^* \, dt \quad . \qquad (16)$$

Using the definition of $M_s(t)$ in eq. (14) gives:

$$P_{TS} = \lim_{T\to\infty} \frac{1}{2T} \int_{-\infty}^{\infty} a(\omega)\, a^*(\omega)\, d\omega \qquad (17)$$

A limiting value for P_{TS} occurs when $M_s(t)$ consists of a unit dc level and a unit amplitude single frequency modulation. In this case,

$$M_s(t) = M(t) \equiv 1 + \sin(\omega t + \omega) \quad . \tag{18}$$

Carrying out the integral in eq. (16) for this modulation gives $P_{ST} = 1.5$.

A more realistic modulation function would include several frequencies with random phases. By increasing the number of frequencies, however, we can never exceed a total average power 1.5. This conclusion can be demonstrated by considering a modulation function with two frequencies:

$$M_s''(t) \equiv 1 + a_1 \sin(\omega_1 t + \phi_1) + a_2 \sin(\omega_2 t + \phi_2) \quad , \tag{19}$$

where a_1 and a_2 are positive, and ϕ_1 and ϕ_2 are random phases greater than zero, but less than 2π. The requirement that $M_s''(t)$ must always be non-negative means $(a_1 + a_2) \leq 1$. Using eq. (16) gives

$$P_{TS} = 1 + \frac{1}{2}(a_1^2 + a_2^2) \leq 1 + \frac{1}{2}(a_1 + a_2)^2 \leq 1.5 \quad . \tag{20}$$

By induction, with N frequencies, P_{TS} can never increase beyond 1.5. Since the dc power is always 1.0, the ac power will never exceed 0.5.

In a multidither COAT servo we are interested only in speckle modulations at or near the dither frequencies, because only they can significantly effect the convergence process. Thus we define a "speckle coefficient", C_s, as

$$C_S \equiv \left\{ \sum_{\pm\omega_i} \int_{\omega_i - \Delta\omega}^{\omega_i + \Delta} \frac{a^2(\omega)}{2T} \, d\omega \right\}^{\frac{1}{2}} \quad . \tag{21}$$

This coefficient is the sum of 2N integrals, where N is the number of dither frequencies in the COAT servo. The summation is carried out over both positive and negative values of the dither frequencies, ω_i. The quantity $\Delta\omega$ is the open loop, unity-gain bandwidth of each COAT servo channel. These quantities are shown graphically in Fig. 23 for the positive half of the power spectrum of an arbitrary modulation function. The shaded areas correspond to the integrals in eq. (21), while the total area under the curve (including the negative frequencies) corresponds to the integral in eq. (17).

Physically, C_s^2 corresponds to that portion of the ac modulation power in $M_s(t)$ which is at or near enough to each dither frequency such that it can create false error signals which compete with the correct dither signals for control of the convergence process. Clearly, the sum of the integrals in eq. (21) will always be less than or equal to the integral in eq. (17). In physical terms, this is the obvious statement that the portion of the ac speckle modulation power at or near the dither frequencies is always less than or equal to the total ac power. Since the total ac power is less than or equal to 0.5, then C_s^2 must also be less than or equal to 0.5. Thus

$$C_s \leq \sqrt{0.5} = 0.707 \quad . \tag{22}$$

One must be careful not to confuse the power in the speckle modulation function $M_s(t)$ (i.e., eqs. (16) and (17)) with the speckle signal power calculated in the statistical analysis. The former does not, by itself, represent a physical energy rate. It is just a dimensionless amplitude function which modulates the usual "no-speckle" intensity at the receiver. The latter refers to an actual electric signal within the COAT servo which falls within the control bandwidth. It is directly proportional to C_s^2 and the square of the mean intensity incident on the receiver as shown in (eq. (26)).

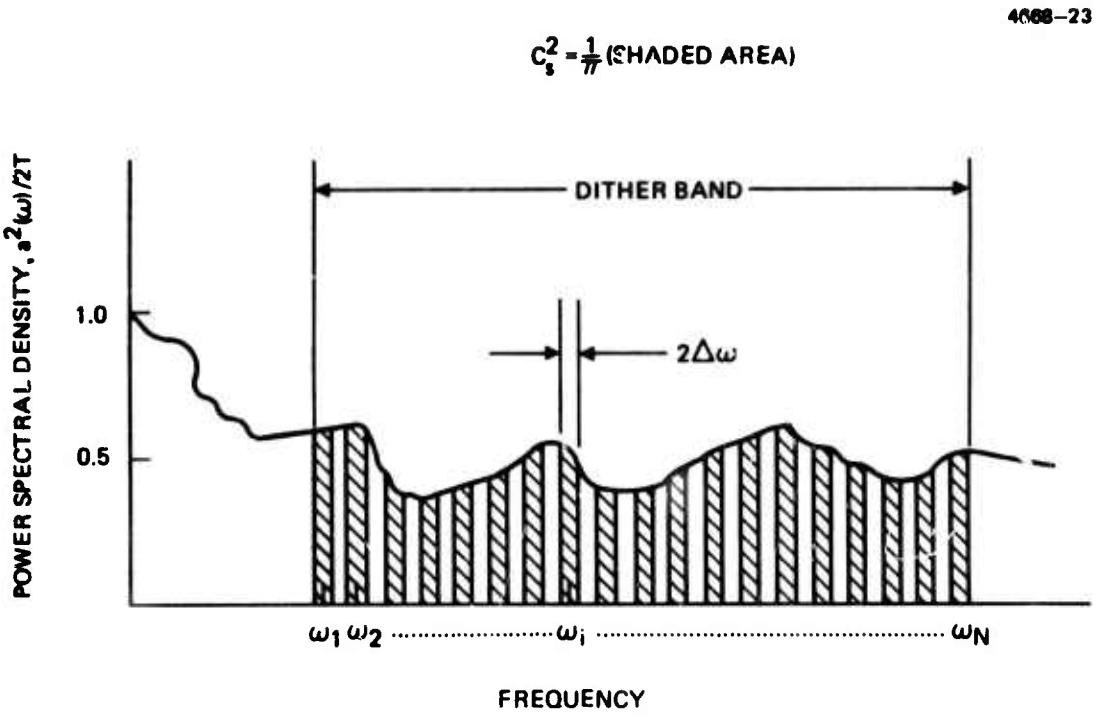

Figure 23. Power spectrum of an arbitrary modulation function.

The generalization of the statistical analysis, as described above results in new expressions for the servo dither signal, S_D, and the servo speckle signal, S_S:

$$KI_D = KI_D \tag{23}$$

$$S_S = M_{ac} KI_m \quad . \tag{24}$$

Both S_D and S_S represent physical voltages, with the following definitions:

$K \equiv$ photomultiplier constant

$I_M \equiv$ mean "no-speckle" intensity at receiver

$I_D \equiv$ dither modulations at receiver

$M_{dc} \equiv$ average value of $M_s(t) = 1.0$

$M_{ac} \equiv$ ac part of $M_s(t)$ at or near dither frequencies.

The rest of the analysis continues in the same manner as before.[5,6] We find the average power in the dither signal, P_D, and the average power in the speckle induced signal, P_S, by calculating the expectation value of the squares the voltages S_D and S_S. The results of these calculations are given in eqs. (25) to (28).

$$\langle P_D \rangle = \frac{1}{2T} \int_{-T}^{T} \langle S_D^2 \rangle \, dt = K^2 \langle I_D^2 \rangle \quad ; \tag{25}$$

$$\langle P_S \rangle = \frac{1}{2T} \int_{-T}^{T} \langle S_S^2 \rangle \, dt = \frac{1}{2T} K^2 \langle I_M^2 \rangle \int_{-T}^{T} M_{ac}^2 \, dt$$

$$= K^2 \langle I_M^2 \rangle C_S^2 \quad , \tag{26}$$

where

$$\langle I_D{}^2 \rangle \equiv 4\left[J_0(\psi)\ J_1(\psi)\right]\left\{\left(\frac{1}{N} - \frac{3}{N^2} + \frac{2}{N^3}\right)\frac{\sin^2\left(\frac{\alpha}{2}\right)}{\left(\frac{\alpha}{2}\right)^2}\left[1 - \frac{\sin\alpha}{\alpha}\right]\right.$$

$$\left. + \left(\frac{1}{N^2} - \frac{1}{N^3}\right)\left[1 - \frac{\sin^2\alpha}{\alpha^2}\right]\right\} \quad ; \qquad (27)$$

$$\langle I_M{}^2 \rangle = \frac{1}{N^2} + 2J_0{}^2(\psi)\left[\frac{1}{N} - \frac{1}{N^2}\right]\frac{\sin^2\left(\frac{\alpha}{2}\right)}{\left(\frac{\alpha}{2}\right)^2}$$

$$+ J_0{}^4(\psi)\left[\left(1 - \frac{6}{N} + \frac{11}{N^2} - \frac{6}{N^3}\right)\frac{\sin^4\left(\frac{\alpha}{2}\right)}{\left(\frac{\alpha}{2}\right)^4}\right.$$

$$+ 2\left(\frac{1}{N} - \frac{3}{N^2} + \frac{2}{N^3}\right)\frac{\sin^2\left(\frac{\alpha}{2}\right)}{\left(\frac{\alpha}{2}\right)^2}\left(1 - \frac{\sin\alpha}{\alpha}\right)$$

$$\left. + \left(\frac{1}{N^2} - \frac{1}{N^3}\right)\left(1 - \frac{\sin^2\alpha}{\alpha^2}\right)\right] \quad , \qquad (28)$$

and where

ψ = dither amplitude in radians

N = number of dither channels

α = the angle characterizing the convergence level in the statistical model[5]

$J_i(\psi)$ = the i^{th} Bessel function.

Figure 24 shows the analytically predicted maximum and minimum mean convergence levels as a function of the speckle coefficient C_s. As shown elsewhere,[5] the convergence level oscillates between two well defined levels. It should be pointed out that these analytical predictions represent the minimum performance that can be expected from an 18-channel multidither COAT array that has dither amplitudes of 0.349 radians ($\pm 20^\circ$) in each channel. There are a number of techniques which are mentioned later in this report, and which are still under investigation, that will considerably improve this predicted behavior.

B. Computer Simulations

During the past quarter we received from the General Research Corporation, three computer-generated time functions representing receiver amplitude modulations due to speckle through an arrangement coordinated by the contract monitor Robert Ogrodnik. The three functions were generated by computing the intensity of radiation incident on a point receiver as a function of time. The incident radiation was modeled to correspond to the reflected radiation from a spherical target (1 meter radius) illuminated uniformally over a 10 cm diameter spot by a coherent 10.6 μm source. The receiver is co-polarized with the transmitter and 2 km away from the target. When the target rotates, a speckle pattern sweeps by the receiver causing amplitude fluctuations as a function of time. Thus the normal receiver signal containing the dither modulations is multiplied by another modulation function representing these amplitude fluctuations as shown in the schematic in Fig. 25.

In the computer simulations, the normal receiver signal was multiplied by one of the three time functions generated at GRC. The three different functions correspond to three rotation rates: 0.01 rad/sec, 2 rad/sec, and 10 rad/sec. Figures 26 to 28 show time histories and Fourier amplitude transforms of these functions. The time histories have been normalized by dividing the original functions by 5 so that $M_s(t) \leq 1$; the Fourier transforms correspond to the original functions as generated by GRC. The dither band used in the computer simulations is also indicated in the figures.

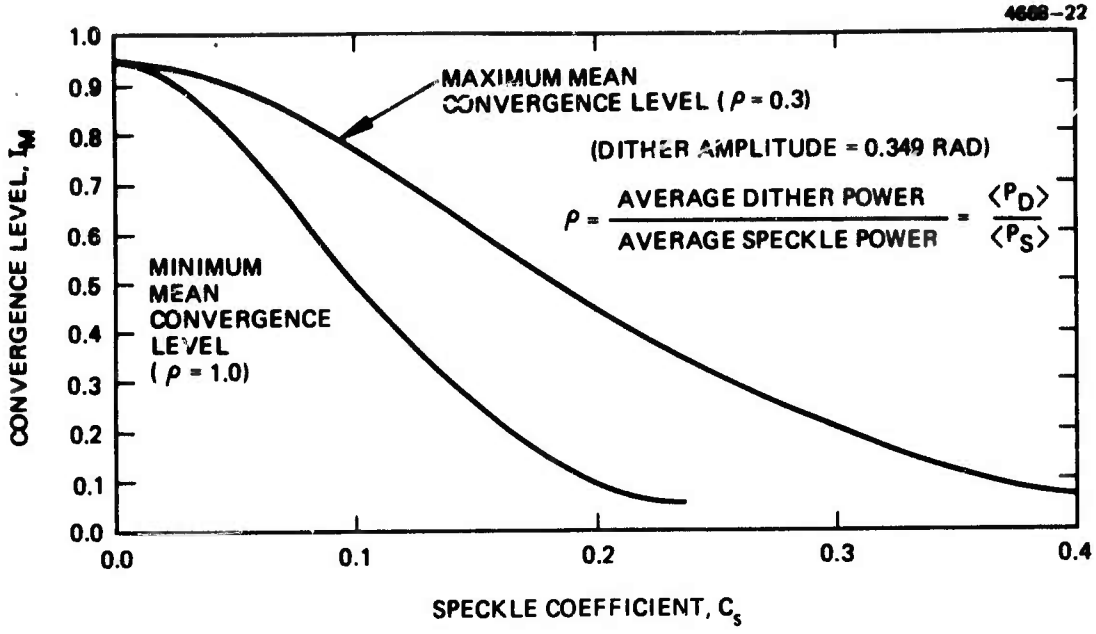

Figure 24. Analytical convergence levels of an 18 element multidither coat array at minimum performance.

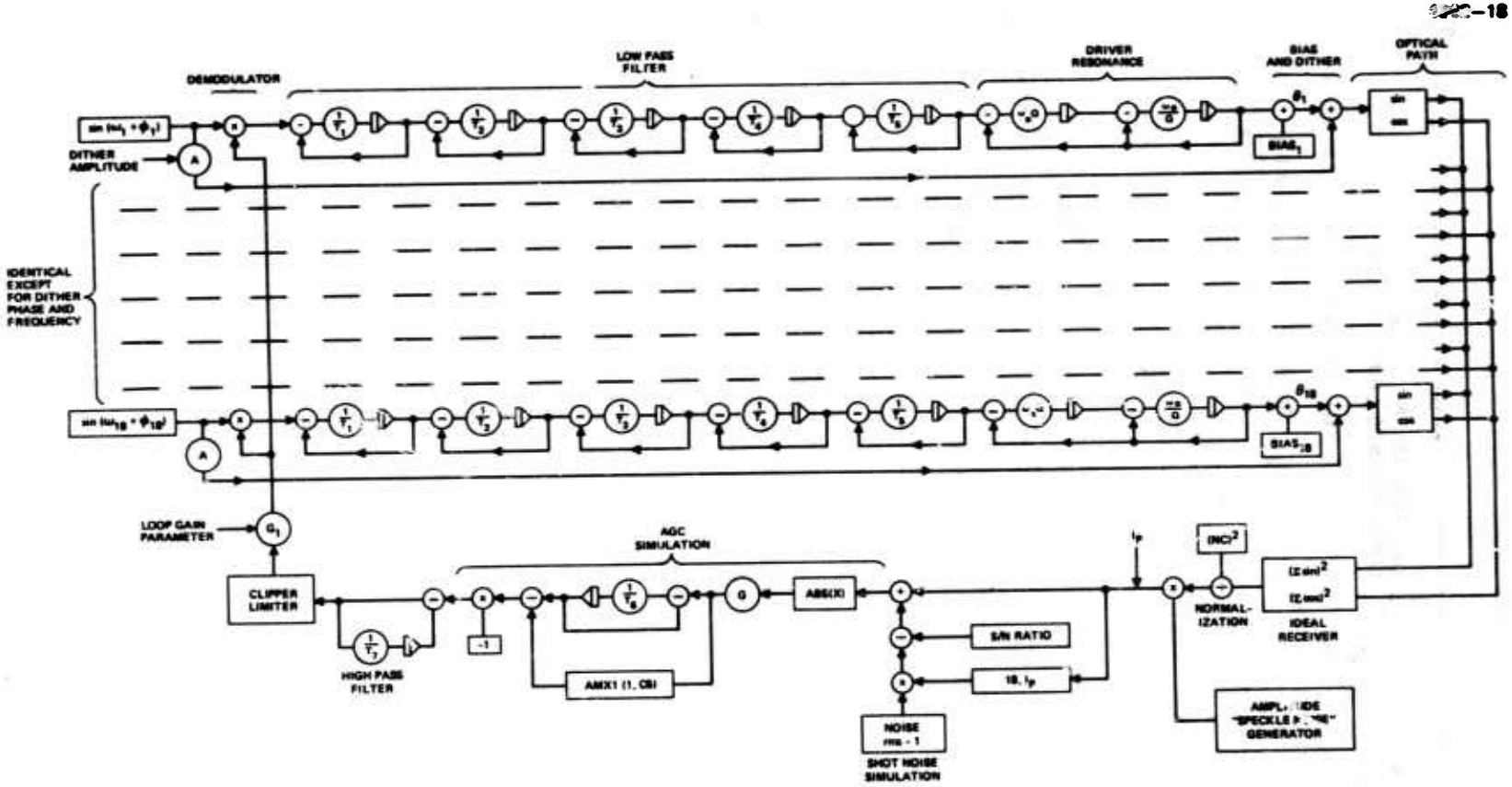

Figure 25. COAT servo simulation showing addition of "speckle" noise generator.

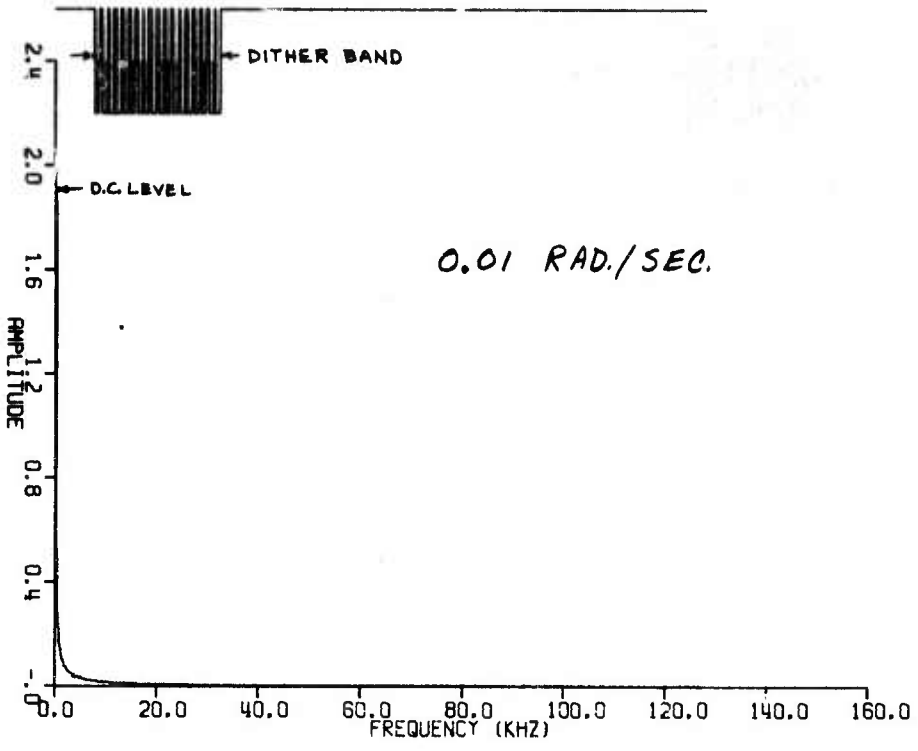

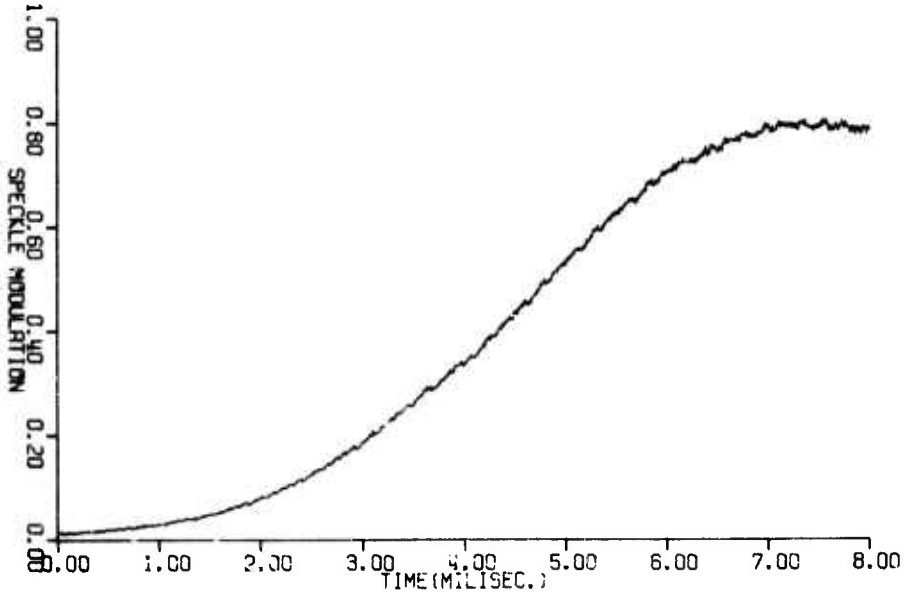

Figure 26. Computer generated speckle modulation function supplied by GRC (Ω = 0.01 rad./sec.).

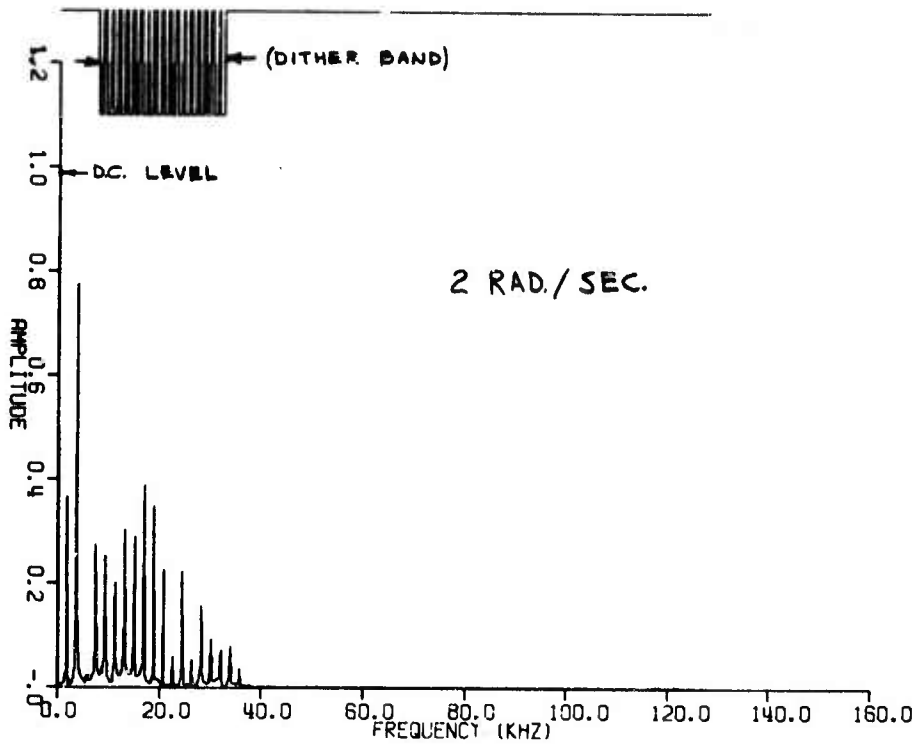

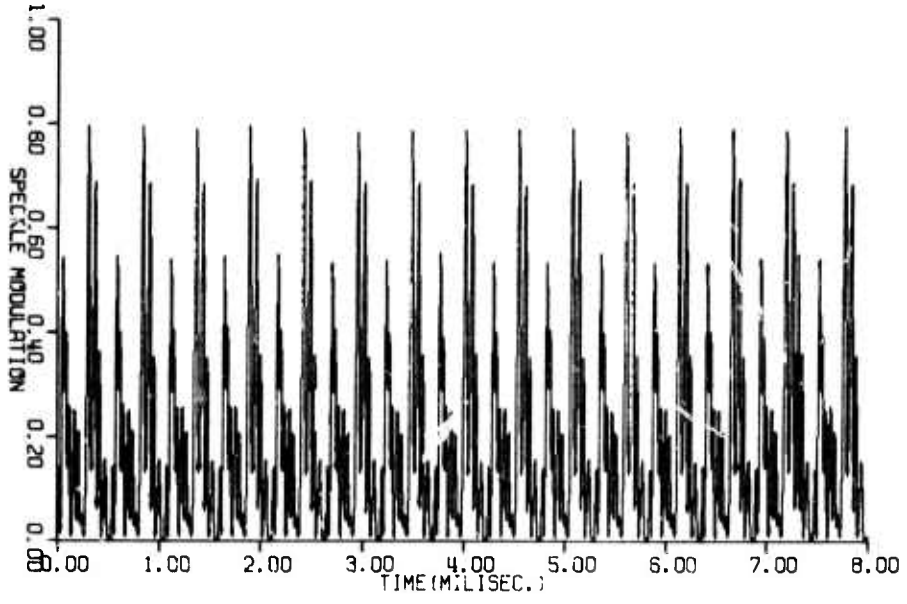

Figure 27. Computer generated speckle modulation function supplied by GRC (Ω = 2 rad./sec.).

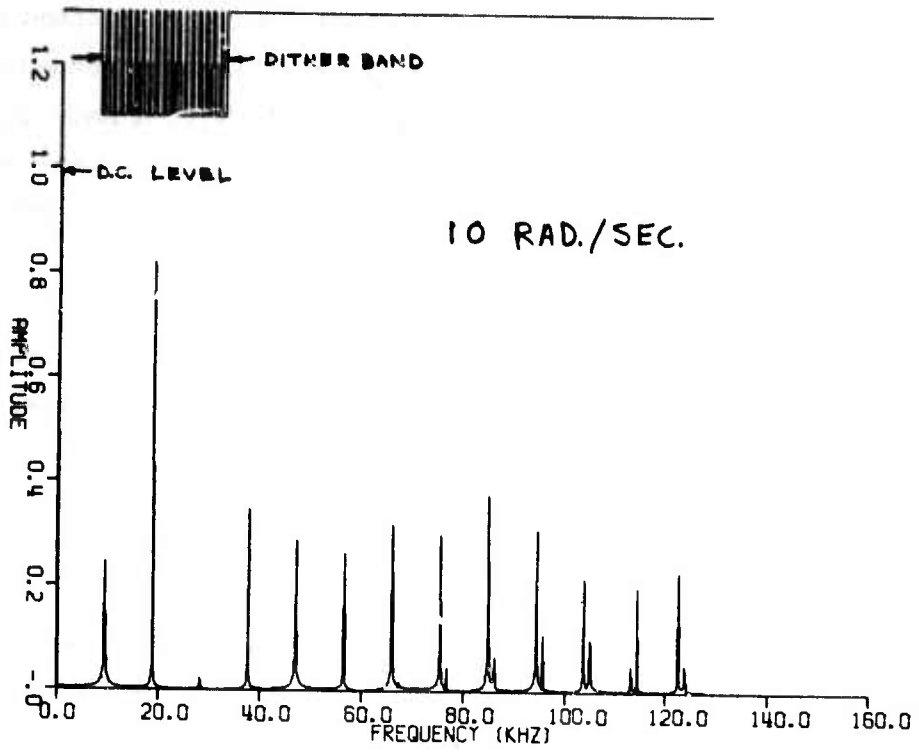

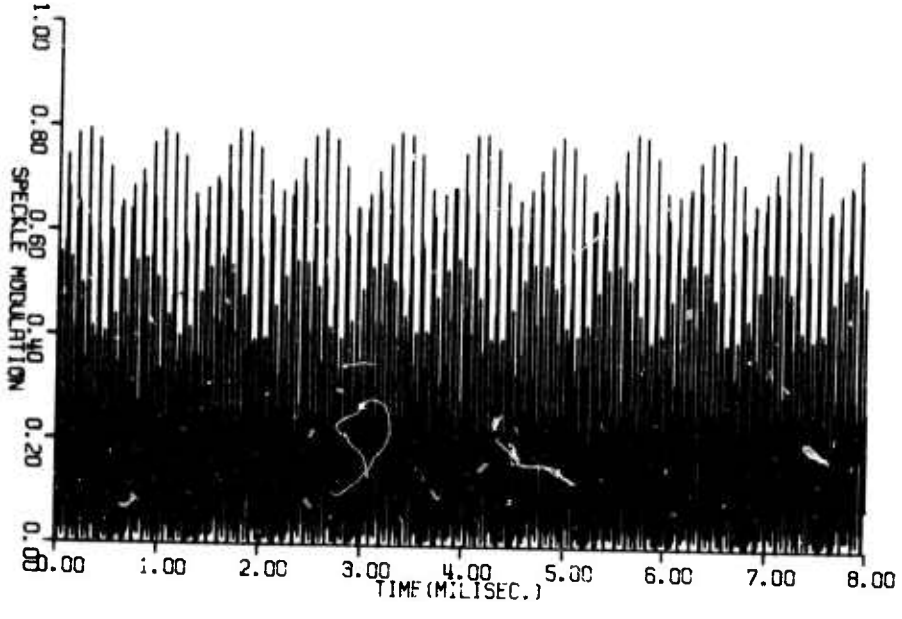

Figure 28. Computer generated speckle modulation function supplied by GRC (Ω = 10.0 rad. sec.).

We have some reservations, which we have communicated to GRC, about how realistic these modulations really are. The first observation is that the modulation functions shown in Fig. 27 and 28 must have been produced by a speckle pattern with a contrast ratio approaching unity because of the very large (essentially 100%) modulation depths. Theoretical and experimental studies done by N. George,[3] together with experimental evidence gathered on this contract and discussed in Section III, indicate that such high contrast ratio speckle patterns are not typically observed at visible wavelengths. Since targets are even more specular at IR wavelengths, it is unlikely that such patterns will be typical at 10.6 μm either. We also note that the modulation functions in Figs. 27 and 28 repeat with a period on order of a 0.5 msec. This is clearly unphysical since the modulations should be a random function of time.

Another reservation we have communicated to GRC concerns the use of a point receiver (i.e. no aperture averaging) in the computation of the modulation function. Realistically, a finite-size receiver will average out some of the intensity fluctuations and thus reduce the effect of high contrast ratios. We are still in the process of resolving these questions at the time of this writing, but we anticipate no difficulty in establishing a mutual consensus between ourselves and the GRC personnel before the end of this contract. The results will be documented in the final report.

A speckle coefficient C_s, was calculated for each of three GRC cases in order to compare them with the predictions made by the statistical analysis. The results are shown in Table 4. The large uncertainty in cases 2 and 3 arises from numerical problems in computing the integrals in eq. (21) for the spectrums in Figs. 27 and 28; it is very difficult to digitally compute the area under a curve that approaches a delta function. A more continuous spectrum would be easier to handle and more realistic as well.

Table 4. Speckle Coefficients of the GRC Supplied Speckle Modulation Functions

	C_s
Case 1. Ω = 0.01 rad/sec	0.04 (±0.02)
Case 2. Ω = 2.0 rad/sec	0.6(±0.05)
Case 3. Ω = 10.0 rad/sec	0.5 (±0.10)

Recall that C_s = 0.707 is the absolute worst possible value consistent with conservation of energy. This corresponds to 100% of the ac power in the speckle modulation functions passing through all the COAT servo filters completely unattenuated. Note that cases 2 and 3 in Table 4 have values of C_s that approach this limit. We therefore conclude that these two cases are very near to the worst possible kinds of modulation functions — realistic or otherwise.

In spite of these reservations, the data supplied by GRC still proved useful. For example, we know that the divider AGC used in the computer simulations does not represent the actual experimental hardware as accurately as we would like. In particular, we have noticed that in simulation runs with very large amplitude, narrow band, speckle modulation functions centered on one dither frequency, there was a definite lack of correlation with experimental data. The simulations always predicted poorer performance. This was attributed partly to the divider AGC, and partly to the signal clipper in the servo loop. Therefore, in order to have any confidence in the computer simulations when using the GRC data, we first had to investigate the problems in the computer simulation. This investigation has shown that the simulation AGC creates a significant second harmonic signal when the speckle modulations approach about 65% modulation depth. We have also been able to demonstrate that stronger signal clipping in the servo loop makes the simulations correlate much better with experiment.

By formulating a better model for the AGC, and by increasing the clipping in the servo loop, we have been able to demonstrate very good agreement between computer-predicted COAT convergence levels and experimentally observed levels. This new configuration is still not optimum, however, since it predicts generally longer convergence times than those observed without these changes. This investigation will therefore continue into the next quarter.

With the above reservations in mind, we now present the results of the computer simulations using the speckle modulation functions generated by GRC. Figures 29 to 31 show time histories of the radiant intensity on a target glint, normalized to unity at maximum intensity, for the case where the target rotation rates are 0.01 rad/sec, 2.0 rad/sec, and 10 rad/sec. These cases represent the best results achieved so far. We expect the COAT system performance to improve when the questions about the AGC and signal clipping raised above have finally been resolved, and when a finite receiver is used in the GRD model.

It is interesting to compare the predictions of the statistical analysis developed under a previous contract[5] (F30602-75-C-0001) and generalized in the previous section of this report, to the computer simulations just discussed. Using the values of C_s in Table 4, we can compare the analytical convergence levels shown in Fig. 24 with those observed in Figs. 29 to 31. We note that the statistical analysis predicts much lower convergence levels for cases 2 (2 rad/sec) and 3 (10 rad/sec), than those observed in Figs. 30 and 31, while in case 1 (0.01 rad/sec) the prediction is about the same as the observed level in Fig. 29. The reason for the agreement or nonagreement varies depending on which case we consider. Case 3 for example, has two narrow-band, high-amplitude frequency modulations within the COAT dither band (see Fig. 28). Since the statistical analysis was based on a random distribution of dither modulations at or near all the dither frequencies, one would not expect accurate predictions for such a spectrum. Cases 1 and 2 have a more continuous spectrum. Thus we would expect better correlation between prediction and observation. Case 1 does show good

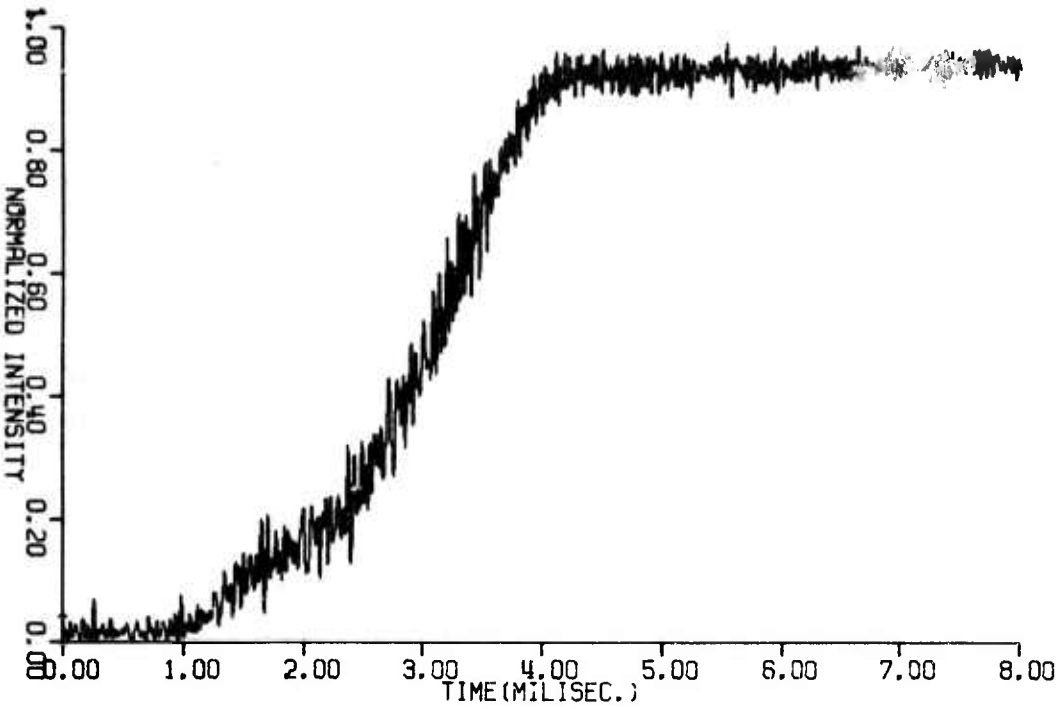

Figure 29. Simulation with GRC modulation function (Ω = 0.01 rad./sec.).

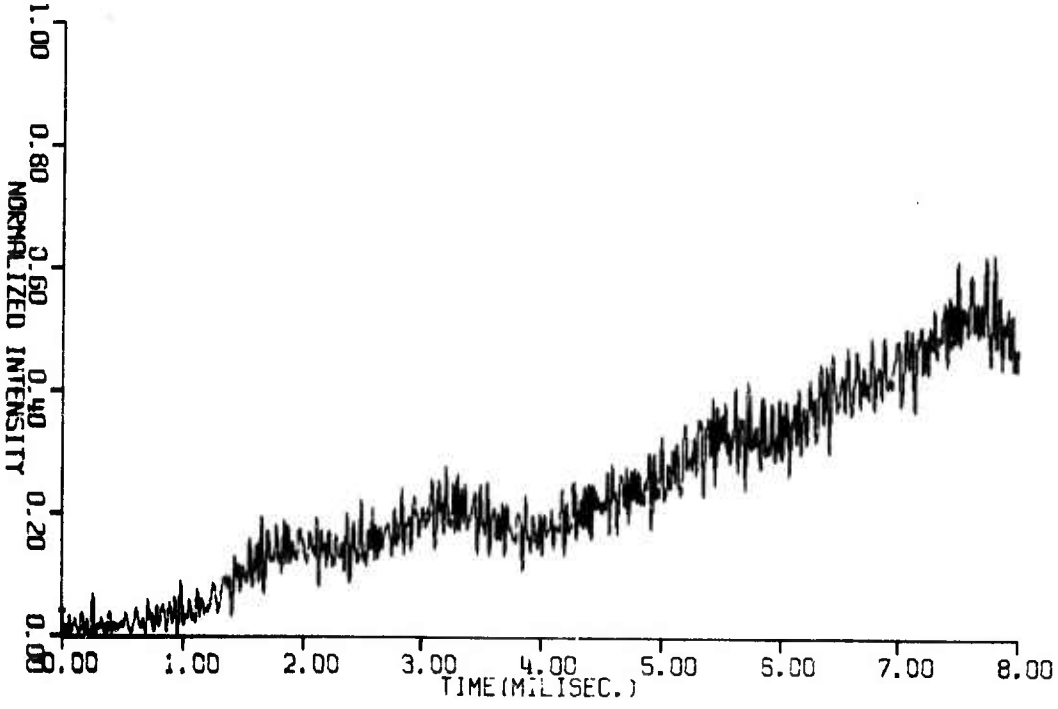

Figure 30. Simulation with GRC modulation with clipping function (Ω = 2.0 rad./sec.).

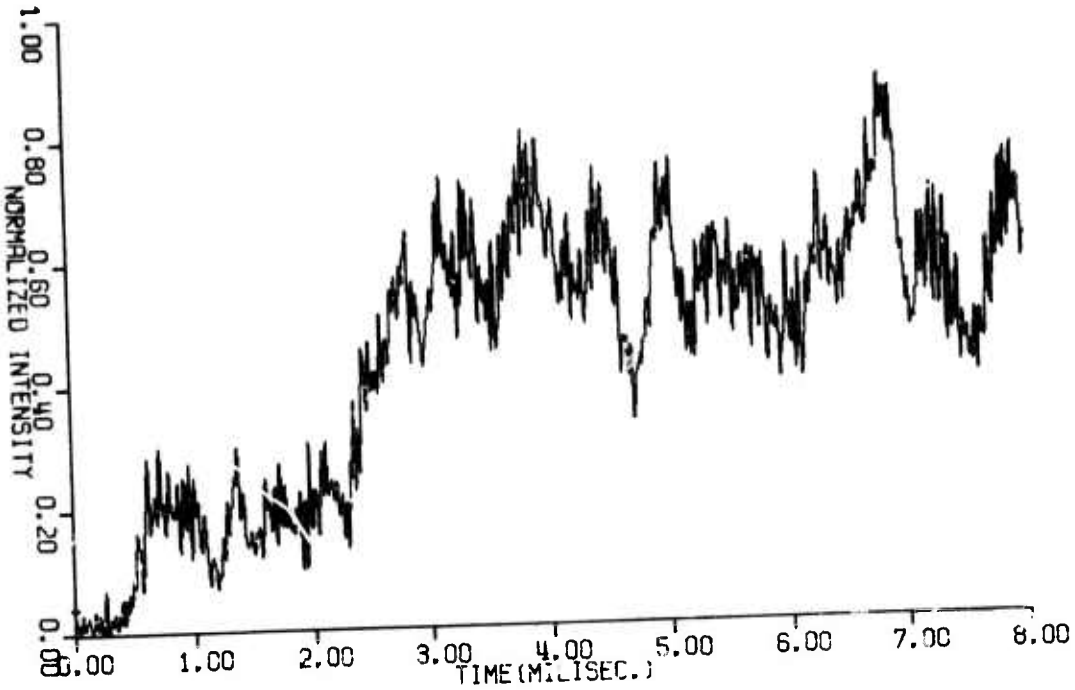

Figure 31. Simulation with GRC modulation function (Ω = 10.0 rad./sec.).

correlation, while case 2 does not. The correlation would be much better in case 2 if signal clipping had not been included in the computer servc loop.

To demonstrate this conclusion, Fig. 32 shows a time history of case 2 (i.e., using the same speckle modulation function as Fig. 36), except that the signal clipping is left out. This case fails to converge at all, which is consistent with the analytical prediction. Since the statistical analysis does not include the effect of signal clipping on the power ratio, we can always expect to improve upon the analytical predictions by including it in the servo.

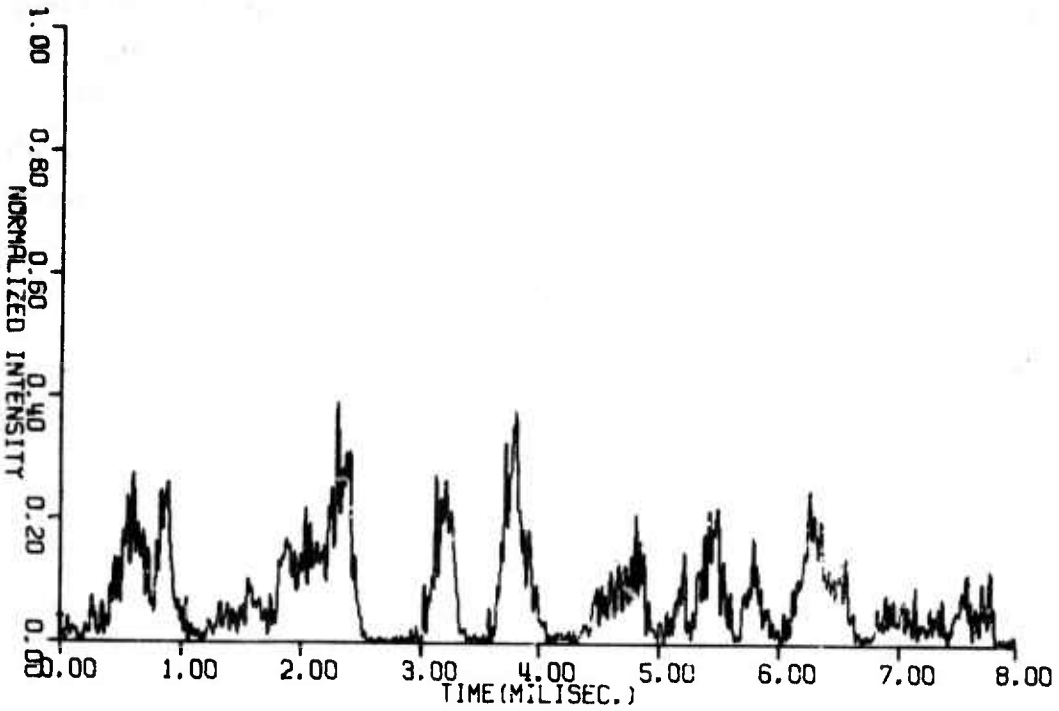

Figure 32. Simulation with GRC modulation function (Ω = 2.0 rad./sec.) (No signal clipping).

V. PLANS FOR THE REMAINDER OF THE PROGRAM

The final contract quarter will be devoted to experimental measurements of COAT system performance with the speckle-characterized targets. The propagation conditions will include turbulence and thermal blooming. Beam convergence level, convergence stability, system convergence time, distortion compensation performance, and tracking performance will be observed. The speckle noise spectrum will be recorded and compared with that obtained from backscatter measurements. An acousto-optic speckle simulation will be performed for the purpose of assessing the minimum modulation index required to overload a single servo channel.

For the computer simulation studies, we will continue to investigate techniques which improve the simulation model response in the presence of speckle noise and also improve its correspondence with the real system. New speckle data to be generated by GRC will be used to test the system response and convergence parameters.

REFERENCES

1. N. George et al "Experiments on the Space and Wavelength Dependence of Speckle", J. Applied Phys., 7, 157-169 (1975).

2. J.M. Burch: In Optical Instruments and Techniques, ed by J. Home Dickson (Oriel Press, Newcastle on Tyne 1970).

3. Private Communication.

4. R.F. Ogrodnik and G. Gurski, "Target Return-Adaptive Aperture System Interaction Effects (U)," 1st DoD Conference on High-Energy Laser Technology, San Diego, CA Oct 1974.

5. J.E. Pearson, et al., "COAT Measurements and Analysis Quar erly Technical Report No. 3," Nov 1975, Contract F30602-75-C-0001, RADC-TR-75-303, (B008 416).

6. J.E. Pearson, M.E. Pedinoff, and S.A. Kokorowski, "Recent Advances in Multidither Coherent Optical Adaptive Techniques (COAT)" Conf. on Laser Engr. and Appl. Phys., Washington, D.C , May 1975, paper 14.9.

MISSION
of
Rome Air Development Center

RADC is the principal AFSC organization charged with planning and executing the USAF exploratory and advanced development programs for information sciences, intelligence, command, control and communications technology, products and services oriented to the needs of the USAF. Primary RADC mission areas are communications, electromagnetic guidance and control, surveillance of ground and aerospace objects, intelligence data collection and handling, information system technology, and electronic reliability, maintainability and compatibility. RADC has mission responsibility as assigned by AFSC for demonstration and acquisition of selected subsystems and systems in the intelligence, mapping, charting, command, control and communications areas.